Second Periodic Report for the Project *"Direct Imaging of Budding and Fusion of Lipid Droplets Mediated by Proteins in Emulsion Droplets Based on Microfluidics - Dynamics of Proteins Interactions, Assembly and Metabolism Energy"*

Brief outcome for the second period

In the last of the BLFD project I had the chance to close two projects triggered during the ongoing phase. My work led to determine the energetics and mechanical regulation of the vesicular trafficking protein machinery complex protein I (COPI) on membranes and to unveil protein crowding as an important mechanism controlling lipid droplet (LD) protein composition. These works fully cover the objectives of the BFLD and led to two scientific publications in Developmental Cell and Plos One.

Scientific accomplishment

Lipid droplets (LDs) are cellular organelles formed by an oil core, essentially made of triglycerides (TG), surrounded by a phospholipid monolayer, and bound by many proteins. LDs serve as cellular energy reservoirs. They are extremely dynamic, a signature of their ability to respond to cellular energy fluctuations. A good regulation of LDs is important otherwise one will develop several kinds of metabolic lipid diseases such as type II diabetes etc. The binding of proteins to LD surface mediates this regulation but the mechanisms leading to their localization to LDs and the control of LD protein composition were not fully understood.

1- The vesicular trafficking protein machinery COPI acts on the Golgi, bounded by a phospholipid bilayer membrane, and on LDs, bounded by a monolayer. I used the microfluidic set up developed during my ongoing phase, presented in my first report and published in Thiam et al. 2013 in PNAS, Fig. 1, to study the energy supplied by the COPI machinery to bud particles from membranes. In the microfluidic device, I generated buffer drops containing COPI in an oil phase. I showed that COPI can assemble at buffer/oil interfaces to bud nano oil droplets of the same size than COPI vesicles, 60 nm, Fig.1. The main results was that COPI is able to form nano droplets only if the buffer/oil was of low surface tension. This was not sufficient to show that surface tension alone opposes budding, as budding could be attributed to the phospholipids. We changed the buffer/oil interface properties by varying the type and concentration of surfactant: we used oleic acid (OA) and dioleoyl glycerol (DOG), both present on LDs in vivo, in combination with phospholipids, Fig. 2. We were able to demonstrate that in this monolayer system surface tension alone controlled budding, Fig. 2. We showed that the COPI budding yield, B_{COs}, follows a Heaviside-like dependency with surface tension. From Fig 2 we deduced the energy of COPI for budding membranes, both bilayers and monolayers, to be 1500-2000k_BT. Knowing this energy allows to understand the ability of cells to remodel their membrane physical properties to allow budding by COPI.

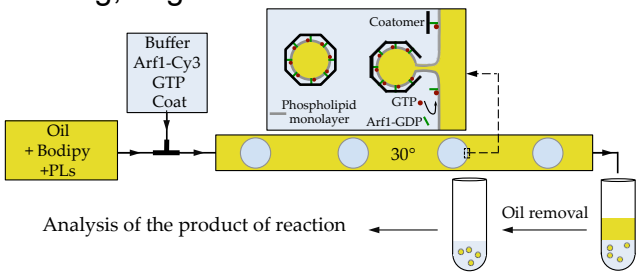

Figure 1: Microfluidic device allowing the formation of buffer drops encapsulating COPI in an oil phase. The inlay is a zoom of the budding process by COPI at the interface.

This work was published in Plos One.
2015 A. Rachid Thiam and Frédéric Pincet: Energy of COPI for budding membranes.

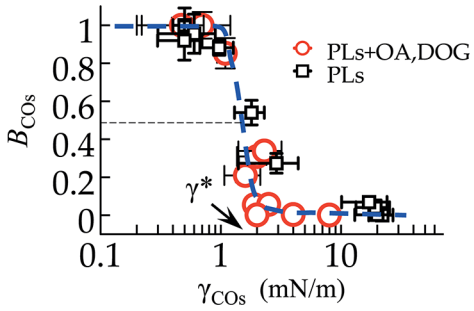

Figure 2: A Heaviside-like evolution of the budding yield B_{COs} against the surface tension.

2- Understanding mechanisms controlling LD protein is important for understanding LD biology. LDs grow and shrink, reflecting the dynamics of cellular energy storage and expenditure. During these steps, proteins can bind or be removed from LDs. During the last year of the BFLD, we have shown that protein crowding is a mechanism that limits the binding of proteins to LDs, especially during LD shrinkage. When LDs shrink, their surface deceases and limits the space for binding. We found that the surface compression stress has a direct consequence on the folding of proteins. Weakly binding proteins will be first expel from the LD surface during shrinkage, kicked off by strongly binding proteins. Fig.4 presents the approach I have developed to demonstrate the protein crowding/competition mechanism as a process controlling LD protein composition. In drosophila cells, we expressed fluorescently tagged LD proteins; the LDs were then purified in an aqueous phase. Water drops containing the purified LDs were formed in oil, as sketched in Fig.4a. Upon mixing, the LDs surface protein content relocated at the interface. This experimental set up offered a zoom of the in vivo LD surface, as the proteins are bound to an aqueous/oil macroscopic interface, which was moreover easily modulated. To mimic in vivo LD shrinkage, we shrunk the water drop formed in the oil phase, Fig.4b top panel (by water evaporation). We looked at two proteins, CCT1 and GPAT4, which were labeled with different fluorophores. During shrinkage, the two proteins in Fig.4b behave differently; CCT1 fell off while GPAT4 stayed at the interface during the shrinkage. The two proteins have different binding motifs. CCT1 binds membranes with an amphipathic helix, which can unfold in the aqueous cytosol, and GPAT4 has a hairpin that strongly tethers it to the membrane interface. With this approach, we competed off different proteins and found that amphipathic-helix binding proteins are mainly expelled form LDs during shrinkage. This finding made us hypothesize that, even without shrinkage, proteins may simply compete for binding LDs due to limited space. To test that, we co-expressed couples of proteins with different tags and expression levels. In Fig 4A is shown an example. As a reference protein, we expressed mCherry-LSD1 at different levels, a protein that strongly bound LDs, and competed it by GFP-tagged version of other LD proteins. We found that elevated expression levels of LSD1 were sufficient to prevent the binding of CCT1 and

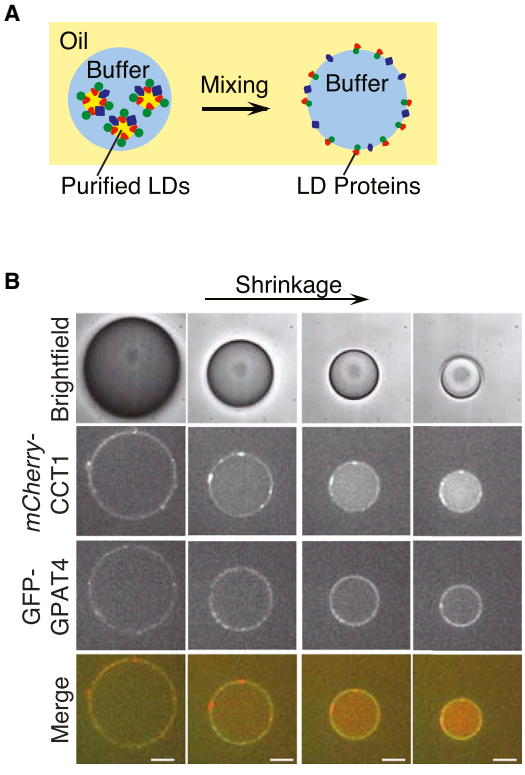

Figure 3: Protein binding competition. a) Principle of relocating LD protein content to the new water/oil interface (water drops formed in oil). b) Two proteins behave differently during water drop shrinkage by water molecules evaporation; one protein falls off while the other stays.

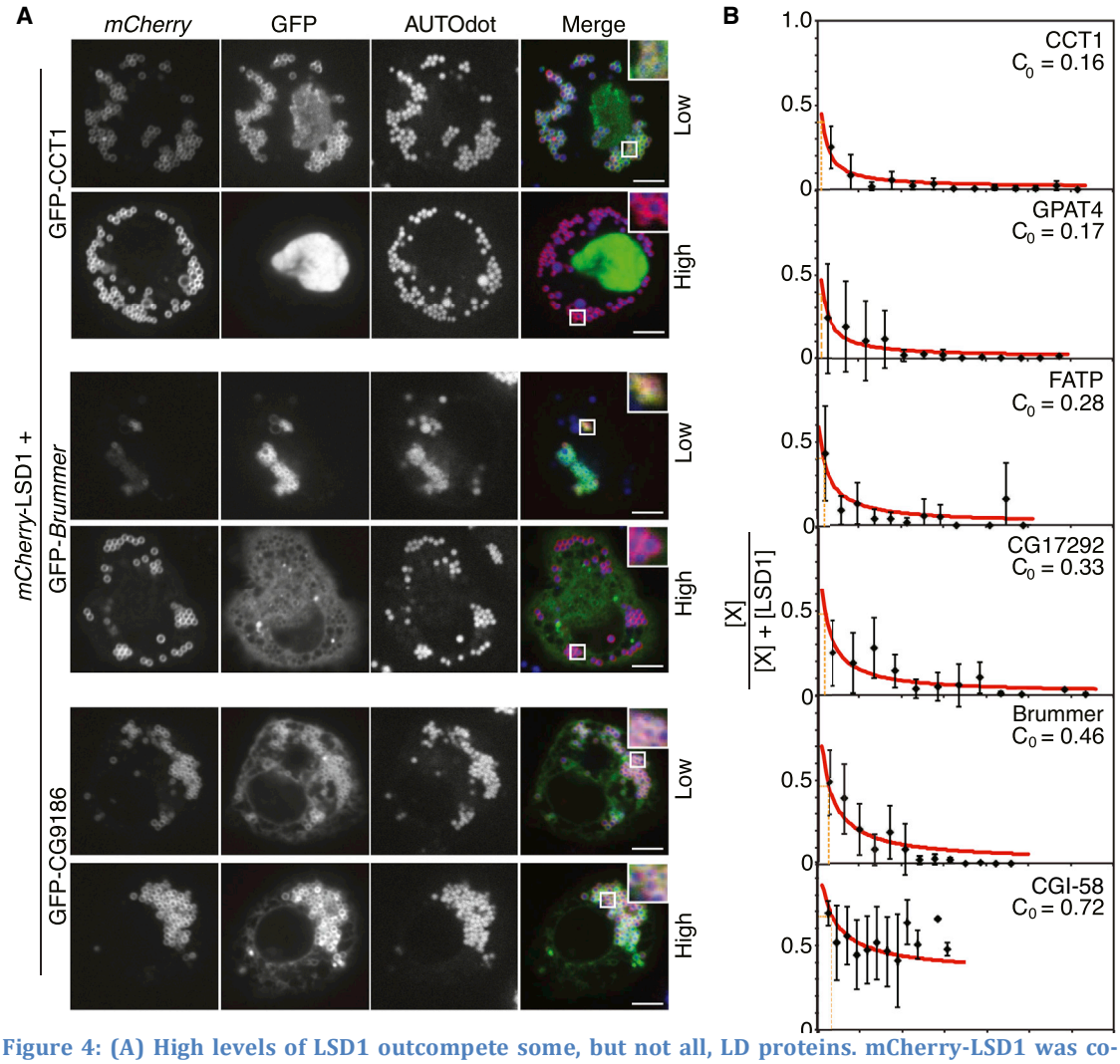

Figure 4: (A) High levels of LSD1 outcompete some, but not all, LD proteins. mCherry-LSD1 was co-expressed with GFP-CCT1 in LD-containing Drosophila S2 cells. One representative cell with low expression (top) and one with high expression of LSD1 (bottom) are shown. LDs were stained with AUTOdot. Scale bar, 5 mm. Inlay: 33 magnification. (B) Some proteins compete more strongly than others against LSD1 at the LD binding surface. Mean fluorescence on LDs ± SD (n > 15).

Brummer to LDs but not of CG9186. At arbitrary concentration, the maximum being 1, 0.16 LSD1 was sufficient to prevent CCT1 binding, 0.46 for Brummer and 0.72 for CG9186, Fig. 4B. These findings were in accordance with the results of the in vitro approach developed in Fig 3 performed with these proteins.
This work was published in Developmental Cell in 2015. 2015 Protein Crowding Is a Determinant of Lipid Droplet Protein Composition

Nora Kory*, **A. Rachid Thiam***, Robert V. Farese, Jr. and Tobias C. Walther, *equal contribution

3- Societal implications of the project

Lipid droplets (LDs) are cellular fat droplets at the core of cellular energy metabolism. Their regulation is crucial for human health. A misfunction of LDs has direct consequences such as the development of cardiovascular diseases and type II diabetes, and many other lipid pathologies including liver steatosis or lipodystrophy. LDs perform many other functions, distinct from the basic regulation or cellular energy metabolism, and serve as hosts for the proliferation of Hepatitis C and Dengue viruses. The fate of LDs and their consequences on human health is based on the specific binding of proteins to their surface. During the three years term of the BFLD project, I tackled important questions of how proteins localize to

lipid droplets (LDs) and how is their binding regulated. This is a main question in the LD field.

Coming from a soft matter background, tackling this question required developing collaboration with biologists, biophysicists and biochemists. I had the opportunity to collaborate with worldwide known cell biologists, experts in LDs, and physiology (Pr. James Rothman at Yale University, USA, Pr. Tobias Walther at Yale also and now at Harvard, MD. Robert Farese at UCSF and now at Havard, USA), biophysicists and biochemists (Pr. Frederic Pincet, ENSParis, France, Dr. Rainer Beck in Heidelberg, Germany, Pr. Bruno Antonny at Sofia, Nice, France). The BFLD project benefited a lot from this pluridisciplinary collaboration; it gave rise to 5 publications, in 3 years, bringing important comprehension of cellular lipid metabolism.

The pluridisciplinary approaches allowed developing various model systems that led for example to unveil the localization mechanisms to LDs of key LD enzymes implicated in fat storage and consumption, which are important process of fat storage during obesity increase and consumption during diet. The mechanisms we found can be modulated to better study, understand lipid metabolism and can allow early intervening for preventing lipid/obesity related pathologies. In plant research, the same mechanisms supposedly occur for LD storage. Since lipids in plants are promising sources of biofuel and food, modulating these mechanisms can improve lipid production.

The mechanisms of LD protein target that I contributed to uncover are now well considered in the field, thanks to publications, but also to the chance I had to present the works during many international conferences (Gordon conference on lipids, FASEB on lipid droplets, New England complex fluids meeting, Eurofed lipids, German Cell Biology conference). Currently, with to the work I did and the opening of my group (thiamlab, www.arthiam.com), I have starting collaborations with many groups in Europe (Cambridge, in England, Dusseldorf, in Germany, Paris, Lyon and Grenoble in France…) that invited me for talks, a good opportunity also for the BFLD work dissemination.

Article

Developmental Cell

Protein Crowding Is a Determinant of Lipid Droplet Protein Composition

Graphical Abstract

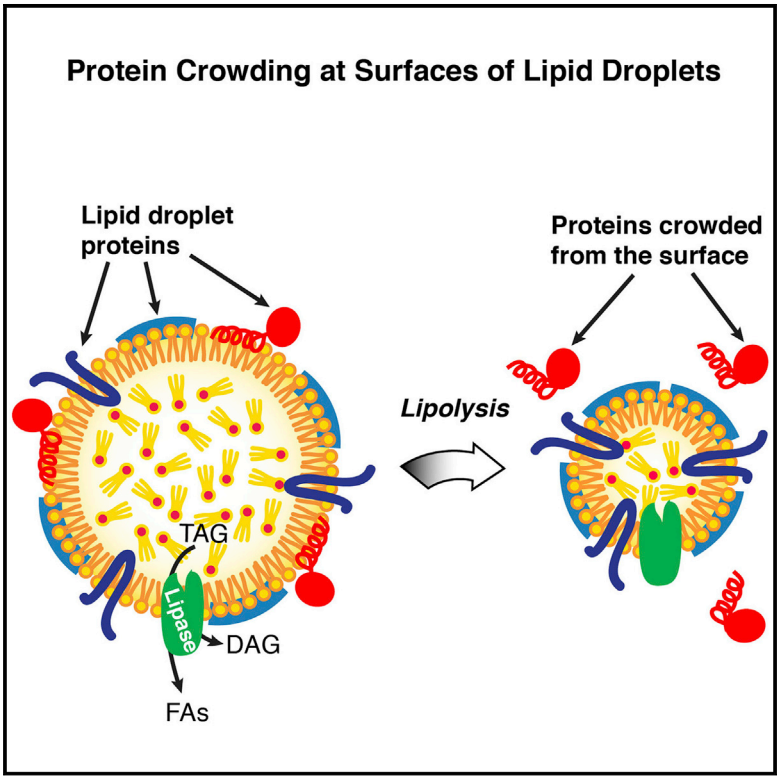

Authors

Nora Kory, Abdou-Rachid Thiam, Robert V. Farese, Tobias C. Walther

Correspondence

robert@hsph.harvard.edu (R.V.F.), twalther@hsph.harvard.edu (T.C.W.)

In Brief

What determines the protein composition of lipid droplets, organelles central to fat storage and metabolism, is unknown. Kory and Thiam et al. identify molecular crowding as a key determinant of lipid droplet protein composition. During lipolysis when lipid droplets shrink, the lipid droplet surface becomes limiting and proteins are selectively displaced.

Highlights

- Molecular crowding is a key determinant of lipid droplet protein composition
- During lipolysis, crowding preferentially displaces some proteins
- Proteins compete for limited binding sites on lipid droplet surfaces

Kory et al., 2015, Developmental Cell *34*, 1–13
August 10, 2015
http://dx.doi.org/10.1016/j.devcel.2015.06.007

CellPress

Please cite this article in press as: Kory et al., Protein Crowding Is a Determinant of Lipid Droplet Protein Composition, Developmental Cell (2015), http://dx.doi.org/10.1016/j.devcel.2015.06.007

Developmental Cell
Article

Protein Crowding Is a Determinant of Lipid Droplet Protein Composition

Nora Kory,[1,2,6] Abdou-Rachid Thiam,[2,3,6] Robert V. Farese, Jr.,[1,4,5,*] and Tobias C. Walther[1,2,4,5,*]
[1]Department of Genetics and Complex Diseases, Harvard T.H. Chan School of Public Health, Boston, MA 02115, USA
[2]Department of Cell Biology, Yale School of Medicine, New Haven, CT 06510, USA
[3]Laboratoire de Physique Statistique, École Normale Supérieure de Paris, Université Pierre et Marie Curie, Université Paris Diderot, Centre National de la Recherche Scientifique, 24 Rue Lhomond, 75005 Paris, France
[4]Department of Cell Biology, Harvard Medical School, Boston, MA 02115, USA
[5]Broad Institute of MIT and Harvard, Cambridge, MA 02142, USA
[6]Co-first author
*Correspondence: robert@hsph.harvard.edu (R.V.F.), twalther@hsph.harvard.edu (T.C.W.)
http://dx.doi.org/10.1016/j.devcel.2015.06.007

SUMMARY

Lipid droplets (LDs) are lipid storage organelles that grow or shrink, depending on the availability of metabolic energy. Proteins recruited to LDs mediate many metabolic functions, including phosphatidylcholine and triglyceride synthesis. How the LD protein composition is tuned to the supply and demand for lipids remains unclear. We show that LDs, in contrast to other organelles, have limited capacity for protein binding. Consequently, macromolecular crowding plays a major role in determining LD protein composition. During lipolysis, when LDs and their surfaces shrink, some, but not all, proteins become displaced. In vitro studies show that macromolecular crowding, rather than changes in monolayer lipid composition, causes proteins to fall off the LD surface. As predicted by a crowding model, proteins compete for binding to the surfaces of LDs. Moreover, the LD binding affinity determines protein localization during lipolysis. Our findings identify protein crowding as an important principle in determining LD protein composition.

INTRODUCTION

Most cells store neutral lipids, such as triglycerides (TGs) and sterol esters, in cytoplasmic organelles called lipid droplets (LDs) (Beller et al., 2010; Greenberg and Coleman, 2011; Walther and Farese, 2012). LDs are dynamic: their sizes depend on the metabolic state and therefore continually change. When lipids, such as fatty acids or sterols, are in excess, they are converted to neutral lipids and are stored in new or expanding LDs. Conversely, when cells require lipids for metabolic energy or membrane components, they catabolize neutral lipids from these organelles by lipolysis (Zanghellini et al., 2008; Zechner et al., 2009), resulting in LD shrinkage (Paar et al., 2012).

LDs are bounded by a surface monolayer, composed primarily of phospholipids and proteins. Many of these proteins mediate lipid metabolism (Athenstaedt et al., 1999; Brasaemle et al., 2004; Fujimoto et al., 2004; Krahmer et al., 2013; Pol et al., 2014). These include enzymes of TG synthesis (e.g., glycerol-3-phosphate acyltransferase 4 [GPAT4] and acyl CoA:diacylglycerol acyltransferase 2 [DGAT2]) (Athenstaedt and Daum, 1997; Kuerschner et al., 2008; Stone et al., 2006; Wilfling et al., 2013), TG lipolysis (Grönke et al., 2005; Kurat et al., 2006; Zimmermann et al., 2004) (e.g., ATGL/Brummer), and phosphatidylcholine (PC) synthesis (e.g., CTP-phosphocholine cytidylyltransferase [CCT]). One of these enzymes, CCT, the rate-limiting enzyme for PC synthesis, is activated upon binding expanding LDs, catalyzing increased PC production for coating the growing LD surfaces (Krahmer et al., 2011). Other proteins targeted to the surfaces of LDs include important regulatory proteins, such as perilipin-adipophilin-TIP47 (PAT) proteins and LSD proteins in *Drosophila* (Brasaemle et al., 1997; Greenberg et al., 1991; Wolins et al., 2001, 2006), and proteins that promote LD fusion (e.g., CIDE proteins [Gong et al., 2011; Jambunathan et al., 2011]).

Proteins are targeted to the surface of LDs by at least two distinct mechanisms. Some proteins, including CCT, bind LDs by inserting their amphipathic helices into the surrounding phospholipid monolayer. These protein segments are likely disordered in the aqueous cytosol and become ordered upon binding to the LD surface (Bigay et al., 2005; Cui et al., 2011; Drin et al., 2007; Dunne et al., 1996; Thiam et al., 2013). Other proteins, including GPAT4, DGAT2, and the putative lipase CG9186 (Goo et al., 2014; Thiel et al., 2013), localize to LDs using ER-LD bridges (Jacquier et al., 2011; Wilfling et al., 2013). The localization of each of these proteins is mediated by a hydrophobic membrane-embedded domain that facilitates their delivery from the ER bilayer to the LD surface (Ingelmo-Torres et al., 2009; Wilfling et al., 2013; Zehmer et al., 2008).

Despite increased understanding of how proteins are targeted to the surface of LDs, the mechanisms that determine protein composition of LDs remain unclear. The targeting of some proteins, including hormone-sensitive lipase (HSL), ATGL, CGI-58, and CCT, is regulated by phosphorylation, which is dependent on the cellular metabolic state (Egan et al., 1992; Arnold et al., 1997; Brasaemle et al., 2000; Sahu-Osen et al., 2015; Xie et al., 2014). However, the principles regulating the relative amounts of these and other proteins at LD surfaces are not understood.

LDs possess unusual properties that necessitate distinct protein targeting mechanisms. For example, unlike other organelles bounded by bilayer membranes, LDs consist of a phospholipid

Please cite this article in press as: Kory et al., Protein Crowding Is a Determinant of Lipid Droplet Protein Composition, Developmental Cell (2015), http://dx.doi.org/10.1016/j.devcel.2015.06.007

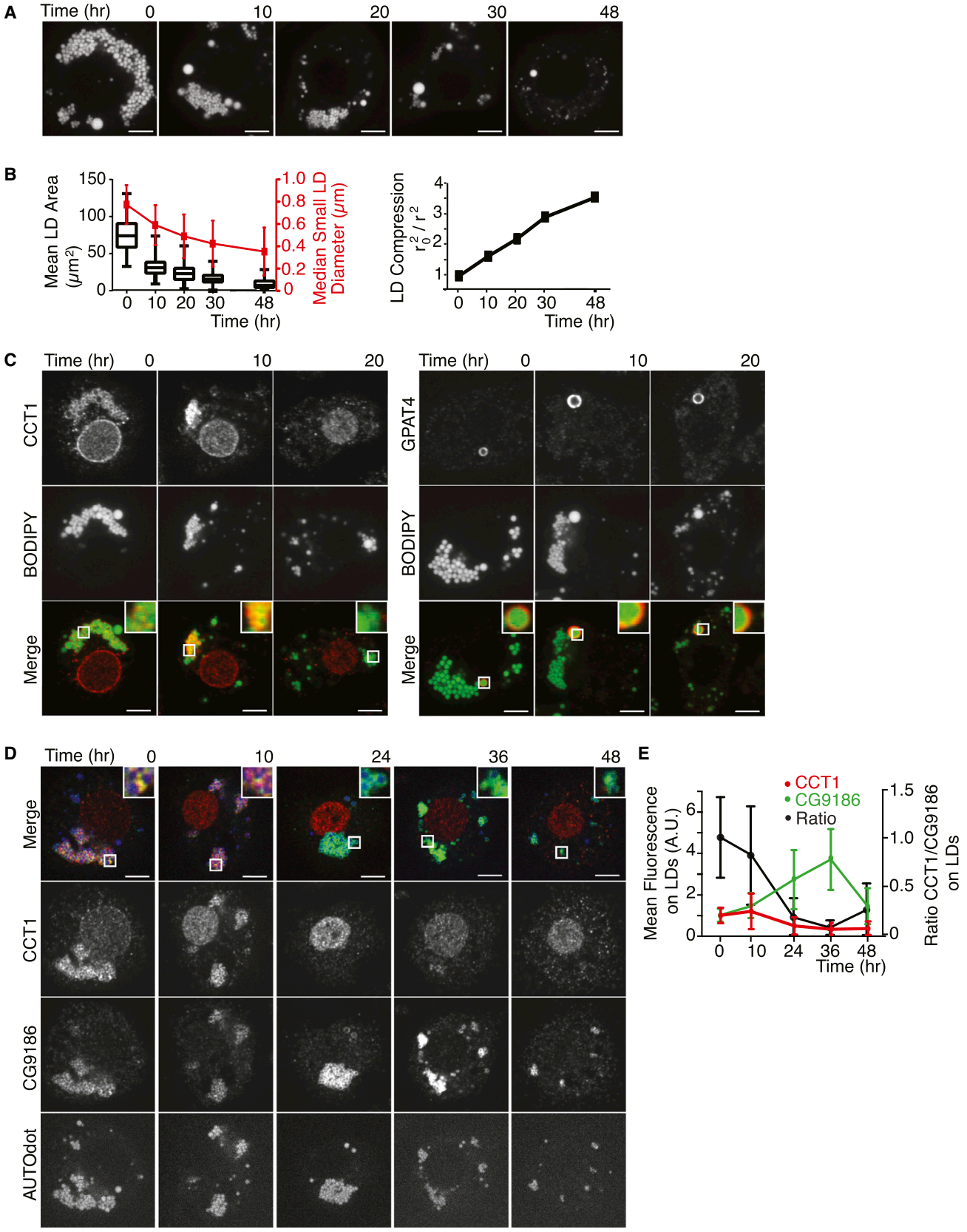

(legend on next page)

monolayer surrounding a neutral lipid core. Therefore, the surface of LDs is unable to accommodate transmembrane proteins with hydrophilic luminal domains. Furthermore, in contrast to other large membranous organelles, such as the ER or Golgi, LDs are discrete entities with only limited binding surfaces. When LDs expand, their surface area increases, providing a platform for additional proteins to bind and mediate aspects of LD growth. For example, CCT normally resides in the nucleus or cytosol but specifically targets expanding LDs when excess fatty acids drive TG synthesis and storage (Krahmer et al., 2011). When LDs shrink during lipolysis, their binding surface decreases. How proteins are removed from LDs when they shrink is unknown.

Here, we investigated mechanisms that determine the protein composition of LDs. Using a combination of cell-based and in vitro reconstitution studies, we uncover macromolecular crowding as a major principle that mediates changes of protein composition of LDs. Our findings suggest that different binding affinities of proteins have evolved to fine-tune the LD protein composition to meet cellular needs.

RESULTS

Lipid Droplet Protein Composition Changes during Lipolysis

We first investigated the localization of LD proteins during lipolysis, which results in marked shrinkage of LD surfaces. To study this process, we incubated oleate-loaded *Drosophila* S2 cells in media lacking lipids, which leads to mobilization of their lipid stores. At the start of the experiment, cells had many LDs smaller than 1 μm in diameter (Figures 1A and 1B). After 48 hr of lipid deprivation, LDs were consumed or decreased dramatically in size (~50% reduction in median diameter), resulting in a ~3.5-fold compression of their surface areas (Figure 1B).

We examined the localization of proteins during LD shrinkage by immunofluorescence, focusing on two proteins that are targeted to LDs by two distinct mechanisms: (1) CCT1, which binds LDs via an amphipathic helix, and (2) GPAT4, which binds via a hydrophobic hairpin motif (Krahmer et al., 2011; Wilfling et al., 2013). Endogenous CCT1 was present on LDs before and after 10 hr of lipid deprivation, but was almost completely absent from LDs after 20 hr, when instead it localized to the cell nucleus (Figure 1C, left). In contrast, endogenous GPAT4 remained on LDs (Figure 1C, right).

To determine whether the localization of other proteins changes during lipolysis, we co-stained the cells with antibodies against CCT1 and CG9186, a putative lipase (Goo et al., 2014; Thiel et al., 2013), during lipid starvation. Like GPAT4, CG9186 has a hydrophobic LD binding motif that is predicted to have a hairpin structure (Thiel et al., 2013). Both CCT1 and CG9186 localized to the same LDs at the beginning of the time course (Figure 1D). As expected, CCT1 was no longer found on LDs between 10 and 24 hr of lipid deprivation (Figure 1D; Krahmer et al., 2011). In contrast, CG9186 increased in concentration 3-fold after 30–36 hr of lipolysis and remained on LDs (Figures 1D and 1E). This increase correlated with a 3-fold decrease in LD surface area (Figures 1B and 1E).

Next, we extended our analyses to a series of proteins that bind LDs by various mechanisms. These included proteins involved in lipolysis, including CG17292, ATGL, and CGI-58, or TG synthesis, such as fatty acid transport protein (FATP). We expressed *mCherry*-tagged forms of these proteins and examined their localization during lipolysis. Each of the proteins localized to LDs at the beginning of the time course (Figure 2A). The binding of some of these proteins, such as CCT1 and CG17292, was strongly reduced after lipid deprivation (81% and 64% reductions, respectively, after 24 hr; Figures 2A and 2B). In contrast, other proteins, such as CG9186 and LSD1, remained mostly bound (34% and 16% reduction, respectively, after 24 hr; Figures 2A and 2B). In general, levels of amphipathic helix-containing proteins such as CCT1 and CG17292 were reduced on LDs during lipolysis, whereas levels of proteins with more hydrophobic LD-binding domains, such as GPAT4, CG9186, or multiple LD-binding motifs, such as LSD1 (Arrese et al., 2008), remained mostly bound (Figure 2B).

CCT1 Falls Off Shrinking Lipid Droplets but Is Not Degraded

We reasoned that CCT is displaced from LDs during lipolysis. However, it is also possible that CCT1 is degraded during lipolysis and newly synthesized CCT1 subsequently is restricted to the nucleus. To rule out this possibility, we generated CCT1 fused to photoactivatable GFP (PAGFP) and locally activated this protein at LDs during lipolysis (Patterson and Lippincott-Schwartz, 2002). During lipid deprivation and LD shrinkage, the pool of fluorescent CCT1 gradually disappeared from the LD surface and appeared in the nucleus (Figures 3A and 3B). In addition, the amount of PAGFP-CCT1 protein was not reduced in the first 10 hr of starvation (data not shown), and total levels of the enzyme increased during 24 hr of starvation (Figure 3C). The results therefore suggest that CCT is displaced from LDs but is not degraded during lipolysis.

CCT1 Displacement from Lipid Droplets Requires Lipolysis

We considered several mechanisms underlying the displacement of CCT1 from LDs during lipolysis. First, changes in the metabolic

Figure 1. During Lipolysis, LDs Shrink and LD Protein Composition Changes

(A) LDs are consumed during lipid starvation. After 48 hr in medium without lipids, LDs shrink and are removed from cells. LDs are stained with BODIPY. Representative images are shown. Scale bar, 5 μm.

(B) LD size decreases during lipid starvation. Mean LD area per cell, median LD diameter of the small LD population, and compression factor (r^2(time 0)/r^2(respective time point); r = radius) during lipolysis are shown. Values are means ± SD or medians as indicated (n > 20).

(C) Endogenous CCT1 detected by immunofluorescence, but not GPAT4, is displaced from LDs during shrinkage. Representative images are shown. Scale bar, 5 μm. Inlay: 3× magnification.

(D and E) Endogenous CCT1 is displaced from LDs during lipid starvation, whereas CG9186 concentrates on LDs. (D) LDs were stained with AUTOdot. Representative images are shown. Scale bar, 5 μm. Inlay: 3× magnification. (E) Mean fluorescence on LDs ± SD (n > 20). A.U., arbitrary units. Note that CG9186 remained bound throughout lipolysis, suggesting that these structures are cytosolic LDs.

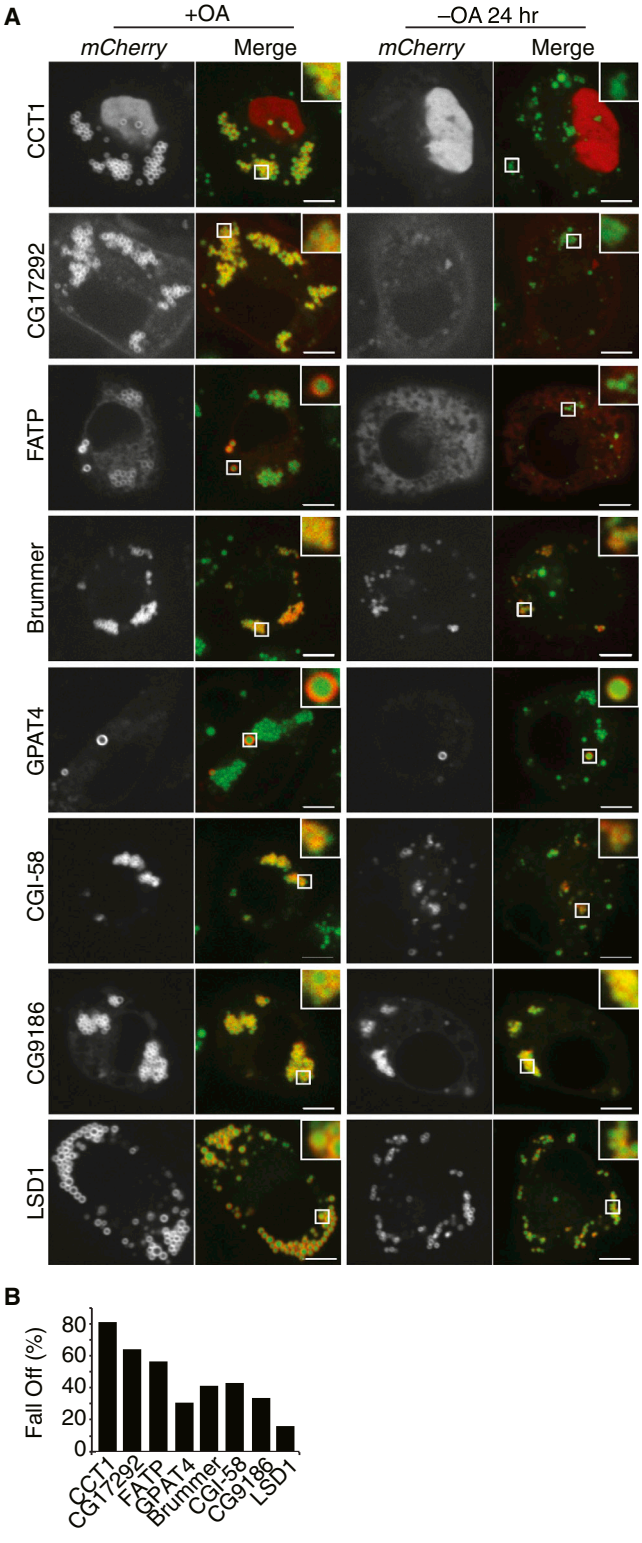

Figure 2. Differential Binding of LD Proteins during Lipolysis

During lipolysis, some proteins are reduced on LDs whereas others remain bound. Cells were imaged after oleate loading (+OA) or after 24 hr (−OA 24 hr) of lipid starvation. LDs were stained with BODIPY.

(A) Representative images are shown. Scale bar, 5 μm. Inlay: 3× magnification.

(B) Percent protein displacement (% protein initially on LDs − % protein on LDs after starvation)/(% protein initially on LDs) is reported. Values are means (n > 12).

state during lipid starvation might activate enzymes that modify CCT1 (e.g., by phosphorylation), changing its binding affinity and localization. Second, changes in lipid composition at the LD surface due to the accumulation of lipid metabolites generated by lipolysis could re-localize CCT to the nucleus. Third, CCT1 could be crowded away from the shrinking LD surface.

To distinguish between these possibilities, we first tested whether lipolysis is required for the re-localization of CCT1 to the nucleus. Blocking lipolysis by the treatment with the lipase inhibitor Orlistat reduced LD shrinkage and prevented CCT1 re-localization (Figures 3D–3F). This suggests that a change of properties at the LD surface, rather than posttranslational modification of CCT1 through the cell signaling of fatty acid starvation, is responsible for CCT1 release. If this is the case, we reasoned that a minimal LD-binding amphipathic helix motif of CCT1 (M-domain; Figure S1A; Krahmer et al., 2011), which is not known to be posttranslationally modified, would be sufficient to exhibit displacement from shrinking LDs. Indeed, we found that the M-domain of CCT1 was released from LDs at a similar rate as wild-type CCT1 during LD shrinkage (Figures S1B and S1C).

Surface Shrinkage Is Sufficient for Displacement of Some Lipid Droplet Proteins

Our results suggest that shrinkage of LDs during lipolysis might be sufficient to preferentially displace some proteins from their surfaces. To evaluate this possibility, we developed an in vitro system using an oil-water interface that recapitulated monolayer shrinkage. We purified LDs from *Drosophila* S2 cells expressing fluorescently tagged LD proteins and mixed them in buffer with an excess of TG. In this system, LD proteins bind to the oil-water interface and can be analyzed by fluorescence microscopy (Figure 4A). Although this system creates an inverse emulsion, the opposite monolayer curvature is irrelevant because the size of these water-in-oil drops (>10-μm diameter), like the size of LD surfaces, is so large that the surface is considered flat on the molecular scale.

Importantly, because the oil phase is experimentally accessible, the influence of different factors at the interface, such as phospholipid concentration, can be tested. To simulate shrinkage of the surface of LDs during lipolysis, water can be evaporated over time from the aqueous drops by adjusting the humidity, leading to shrinkage of the oil-water surface. During shrinkage, the volume of the oil phase remains constant and equilibration of phospholipids between the oil phase and the surface maintains the monolayer lipid composition, allowing the effects of macromolecular crowding from effects of changing surface lipid composition to be independently evaluated.

Using this in vitro system, we evaluated whether shrinkage alone could displace CCT1 from the oil-water interface. We found that during drop shrinkage the CCT1 signal decreased from the interface and concomitantly increased in the aqueous phase (Figures 4B and 4C). In contrast, proteins that stay on

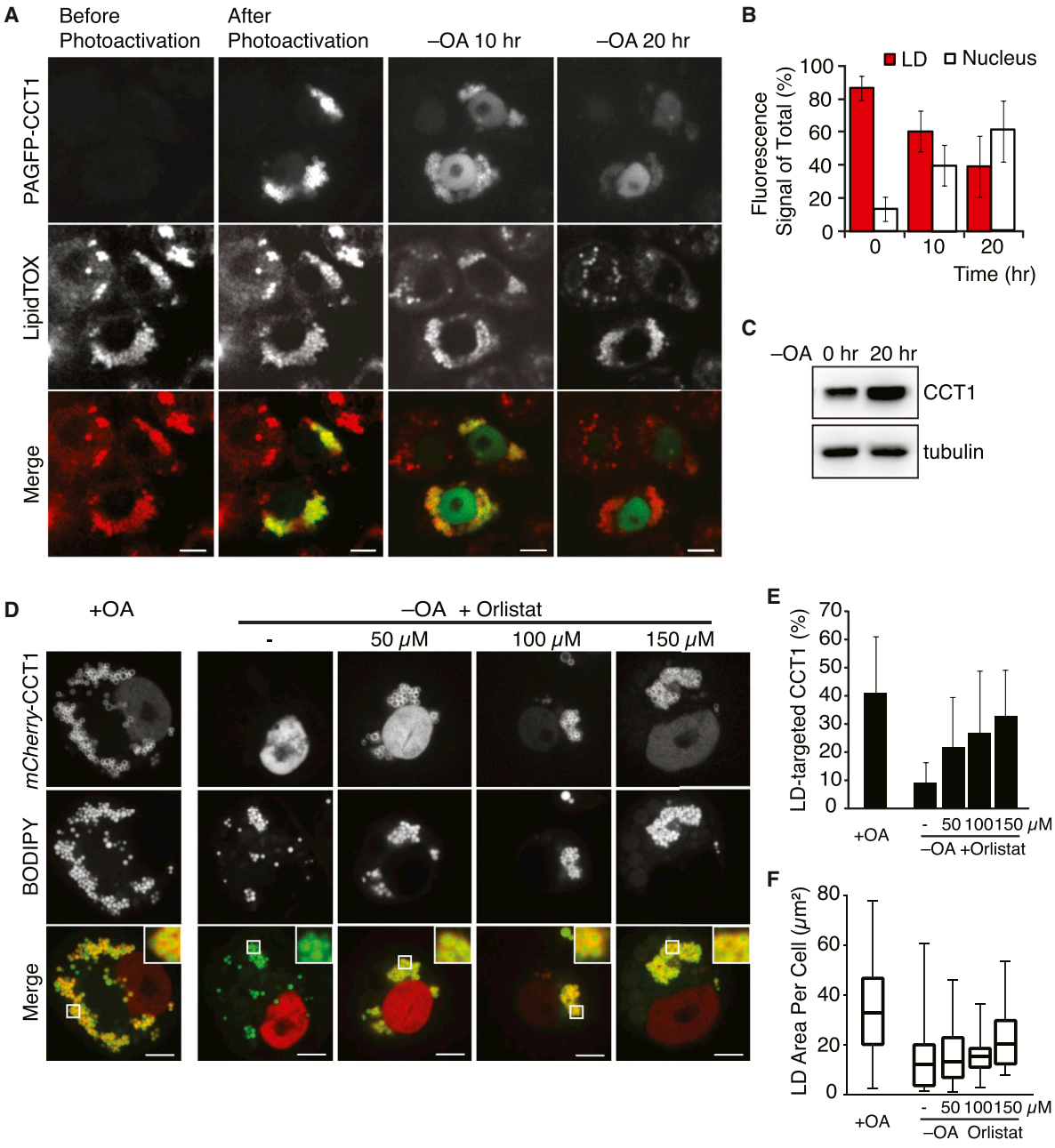

Figure 3. CCT1 Falls Off Shrinking LDs

(A and B) CCT1 is not degraded but falls off LDs when cells are starved for lipids. Photoactivatable GFP (PAGFP)-CCT1 was activated on LDs before starvation. Cells were imaged before, immediately after photoactivation, and after 10 and 20 hr in medium containing delipidated serum (–OA 10 hr and –OA 20 hr, respectively). LDs were stained with LipidTOX. (A) Representative images are shown. Scale bar, 10 μm. (B) Percent mean fluorescence of PAGFP-CCT1 on LDs and the nucleus ± SD (n = 10).

(C) Total CCT1 levels increase during the first 20 hr of starvation. A representative western blot using an antibody against endogenous CCT1 in cell lysates is shown. Tubulin was used as a loading control.

(D–F) Lipase inhibition blocks CCT1 displacement. Cells expressing *mCherry*-CCT1 were oleate loaded, imaged (+OA), or oleate loaded, starved of lipids for 24 hr in the presence of 0–150 μM Orlistat in DMSO, and imaged (–OA). LDs were stained with BODIPY. (D) Representative images are shown. Scale bar, 5 μm. Inlay: 3× magnification. (E) Percent mean fluorescence of *mCherry*-CCT1 on LDs ± SD. Values are means (n > 12). (F) Lipase inhibition prevents LD shrinkage and clearance. A box plot is shown. Mean values of the LD area in one plane of the cell are reported. Whiskers indicate minimum and maximum values.

See also Figure S1.

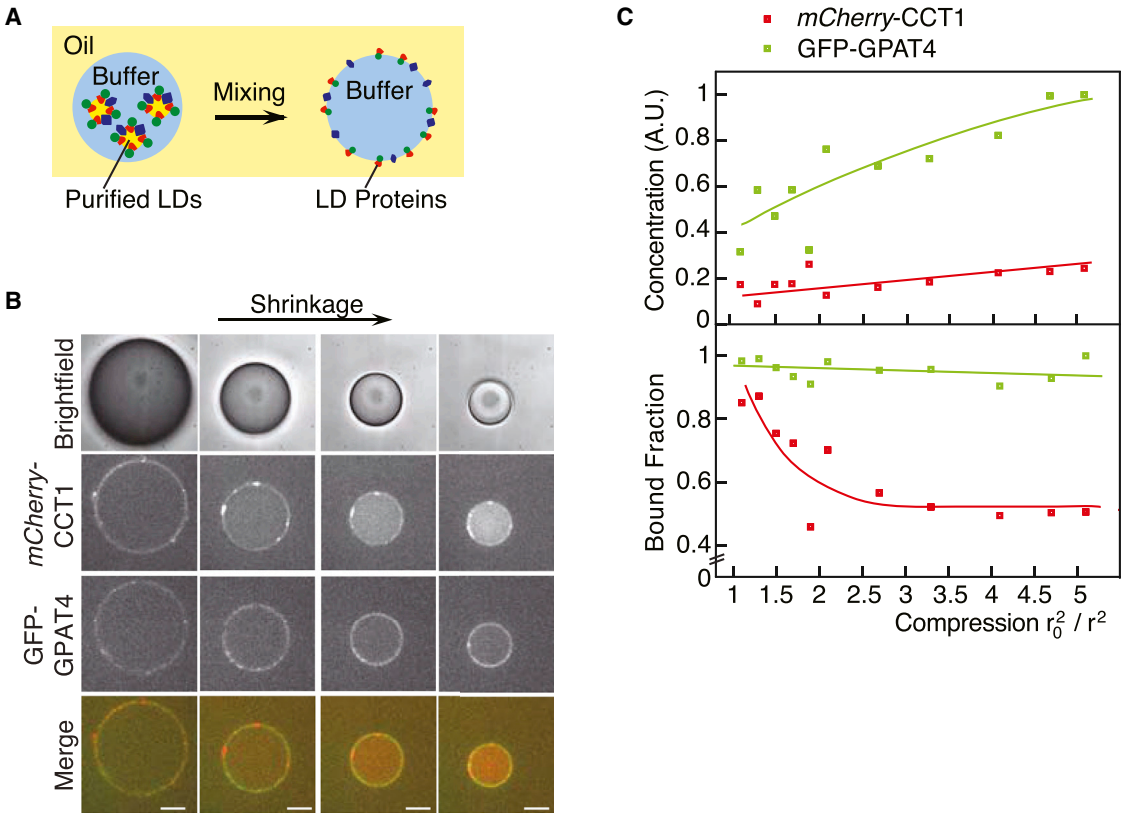

Figure 4. CCT1, but Not GPAT4, Falls Off a Shrinking Oil-Water Interface In Vitro

(A) Schematic of the in vitro system. LDs in buffer are mixed with TG oil to generate a water-in-oil emulsion. LD proteins then bind to the resulting oil-water interface. (B and C) During shrinkage of drops in vitro, CCT1 falls off the oil-water interface, whereas GPAT4 remains bound. (B) Representative images are shown. Scale bar, 10 μm. (C) Surface mean concentration and mean surface-bound fraction for *mCherry*-CCT1 and GFP-GPAT4 are reported. Lines represent trends. A.U., arbitrary units.

See also Figure S2.

shrinking cellular LDs, such as GPAT4, LSD1, or CG9186 (Figures 4 and S2), remained at the oil-water interface and increased in concentration as the surface shrunk. No changes, other than surface shrinkage, were required to recapitulate the displacement of LD proteins from the interface in the in vitro system.

Changes in the Composition of Surface Lipids at Oil-Water Interfaces Are Not Sufficient to Displace Proteins

It is possible that CCT1 might fall off LDs during lipolysis due to changes in lipid composition at the shrinking LD surface. Indeed, during LD expansion, when levels of PC are reduced, CCT1 binds LDs (Krahmer et al., 2011). We therefore tested if increasing the concentration of PC at the shrinking oil-water interface is sufficient to displace CCT1 from the oil-water interface. To test this possibility, we added 25 mM PC to the oil phase, a concentration vastly exceeding its critical micellar concentration in oil (~0.5 mM) or water (nanomolar). This leads to saturation of the oil-water interface, with excess PC predominantly partitioning into the oil phase. Under this condition, and in the absence of drop shrinkage, CCT1 remained bound to the oil-water interface (Figures 5A and 5B). Similarly, adding other lipids to the interface, including either fatty acids, diacylglycerol, monoacylglycerol, a phosphatidylethanolamine (PE)-PC mixture, or a phospholipid mixture mimicking the LD surface composition, did not reduce the amount of CCT1 bound to oil-water interface (Figure S3A). Furthermore, we confirmed that added phospholipids reached the oil-buffer interface (data not shown) by addition of the fluorescent tracer, rhodamine-PE (data not shown). These results indicate that changes in the lipid composition of the interface lipids alone are insufficient to affect binding of CCT1 to the oil-water interface in the in vitro system.

Macromolecular Crowding Mediates Protein Displacement from Shrinking Oil-Water Interfaces

Our results suggest that during shrinkage, LD proteins become crowded at the surface, displacing weakly associated proteins. To test whether the oil-water interface indeed becomes crowded during shrinkage, we used fluorescence recovery after photobleaching (FRAP) to measure the lateral diffusion of proteins on the oil-water interphase before and during drop shrinkage. A slowing of diffusion is the hallmark of macromolecular crowding (Frick et al., 2007; Goose and Sansom, 2013; Han and Herzfeld, 1993; Zimmerman and Minton, 1993). We found that *mCherry*-CCT1 diffused laterally along the interface (Figure 5C).

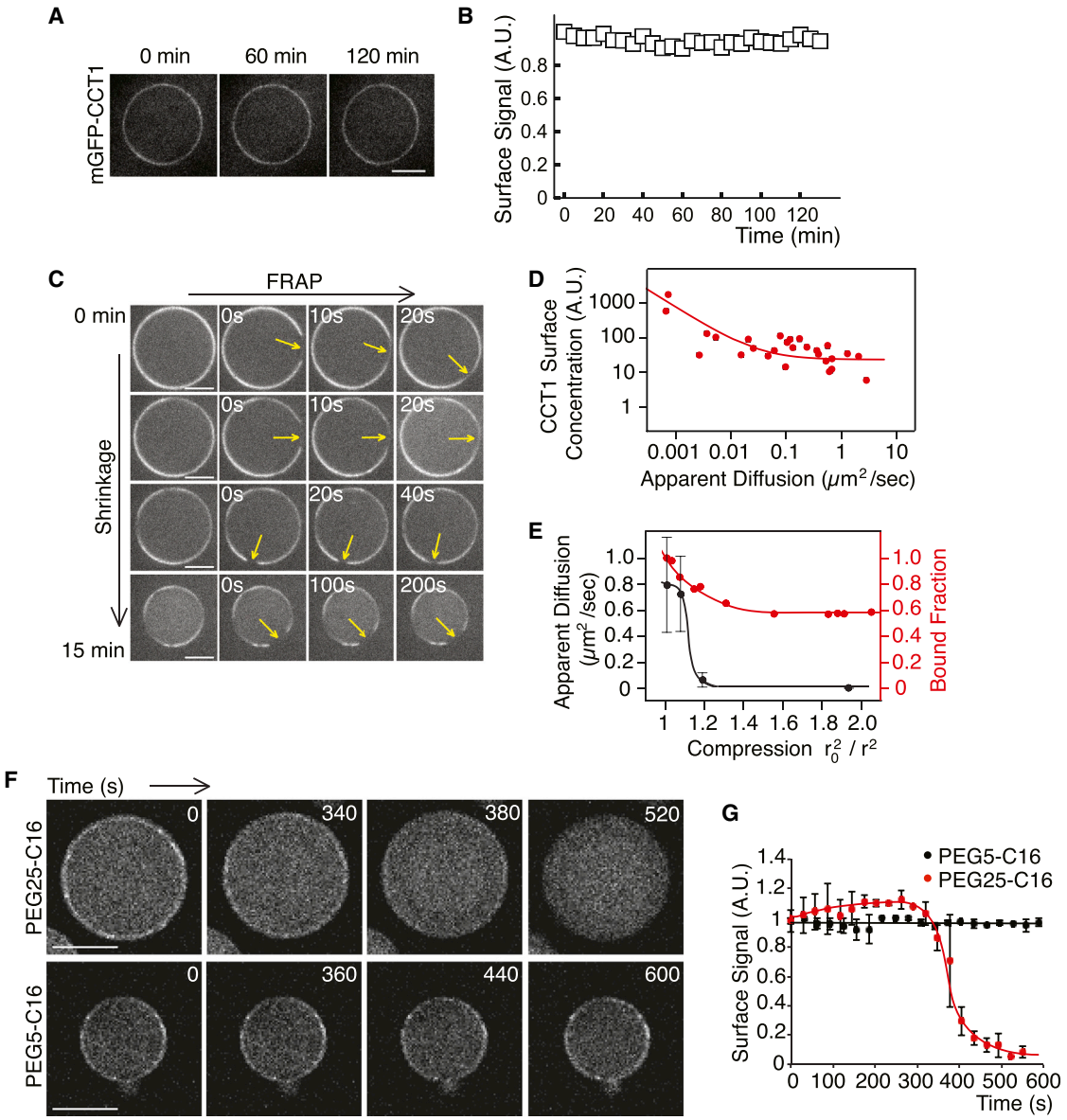

Figure 5. Macromolecular Crowding, Not Changes in PC Concentration, Causes CCT1 Displacement In Vitro

(A and B) PC addition does not affect CCT1 binding to the oil-water interface. Excess PC (2% w/w to TG, 25 mM) was added to the TG oil phase of the inverse emulsion after mGFP-CCT1 was bound at the oil-water interface. (A) Representative images are shown. Scale bar, 10 μm. (B) Mean fluorescence on LDs ± SD (n = 11). A.U., arbitrary units.

(C) Protein diffusion at the oil-water interface of an in vitro drop is gradually decreased upon interface shrinkage according to FRAP analysis. Representative images are shown. Scale bar, 10 μm.

(D) The diffusion of CCT at the oil-water interface is inversely correlated with the concentration of CCT at the drop surface according to FRAP analysis (C). $D \propto 1/C$, assuming a law similar to the Stoke-Einstein law is used to fit the data. Note that shrunken drops have a high concentration of CCT1 at their surface and volume and a low diffusion rate along the surface. A.U., arbitrary units.

(E) CCT1 displacement occurs before its diffusion is limited. Mean diffusion (±SD, n = 4) and a fraction of surface-bound CCT1 were measured on drops and plotted against the compression factor of the drop. Lines indicate trends.

(F and G) High-, but not low-, molecular-weight PEGs crowd out CCT1 from the oil-water interface. PEGs were added at room temperature (2% w/w of the oil) to drops whose interface was bound by mGFP-CCT1. (F) Representative images are shown. Scale bar, 50 μm. (G) Mean mGFP-CCT1 fluorescence ± SD (n = 7) on the drop surface over time is shown. The value at time 0 was normalized to 1. Lines are trend lines. A.U., arbitrary units.

See also Figure S3.

However, under conditions of interface shrinkage, the diffusion rate was dramatically reduced. Importantly, the diffusion rate was inversely correlated with the surface compression factor, with almost no diffusion occurring at a compression factor ≥ 2 (Figures 5C–5E). At extreme compression, the high density of protein led to buckling of the interface (Figure S3B).

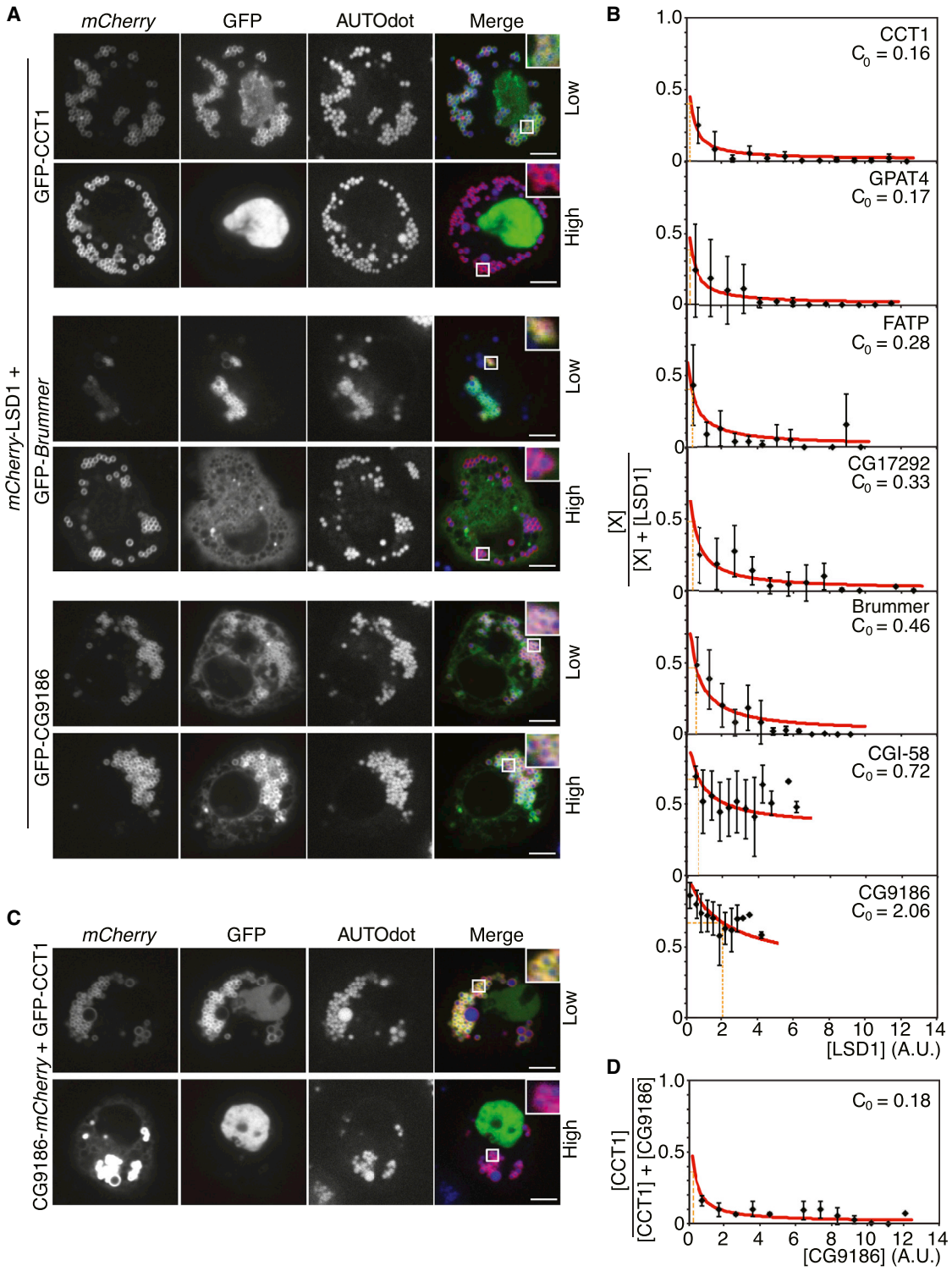

Figure 6. Proteins Compete for Binding at the Lipid Droplet Surface

(A) High levels of LSD1 outcompete some, but not all, LD proteins. *mCherry*-LSD1 was co-expressed with GFP-CCT1 in LD-containing *Drosophila* S2 cells. One representative cell with low expression (top) and one with high expression of LSD1 (bottom) are shown. LDs were stained with AUTOdot. Scale bar, 5 μm. Inlay: 3× magnification.

(B) Some proteins compete more strongly than others against LSD1 at the LD binding surface. Mean fluorescence on LDs ± SD (n > 15). A.U., arbitrary units.

(legend continued on next page)

We reasoned that if macromolecular crowding is responsible for the release of some proteins, such as CCT1, from shrinking oil-water interfaces, the addition of high-molecular-weight polyethylene glycol (PEG), a crowding agent, should produce similar effects. To assess this possibility, we added PEG conjugated to C-16 fatty alcohols in our in vitro system. PEG-fatty acid conjugates are widely used for binding oil-water interfaces to stabilize emulsions and are known to diffuse to these interfaces to fully cover them (Wheeler et al., 1994). As predicted, adding PEG25-C16 displaced CCT1 from the oil-water interface without drop shrinkage at room temperature (Figures 5F and 5G). In contrast, adding a smaller molecule, PEG5-C16, at the same concentration had no effect.

Proteins Compete for Binding the Lipid Droplet Surface

If crowding displaces weakly associated proteins from the shrinking surface during lipolysis, we hypothesized that increasing levels of a protein with high LD binding affinity would change the LD protein composition at a steady state. To test this prediction, we established competition assays in *Drosophila* S2 cells under conditions in which LDs are abundant at a relatively steady state. In brief, we co-expressed a series of LD proteins, together with LSD1, in *Drosophila* S2 cells. Under these conditions, *mCherry*-LSD1 was predominantly localized to LDs in all experiments (80% when co-expressed with CCT1; Figures 6A and S4D). In contrast, increased levels of *mCherry*-LSD1 resulted in decreased levels of most GFP-tagged proteins on the surface of LDs (Figure 6A; Figure S4A). However, some proteins, such as CG9186 (Figure 6A) and CGI-58 (Figures 6A and S4A), were unaffected.

Using these results, we estimated the relative binding affinities of different proteins for the surface of LDs (see Experimental Procedures). Among the proteins tested, CCT1 was most easily displaced by LSD1 ($C_0 = 0.16$), followed by GPAT4 ($C_0 = 0.17$), FATP ($C_0 = 0.28$), CG17292 ($C_0 = 0.33$), and Brummer ($C_0 = 0.46$). CGI-58 ($C_0 = 0.72$) and CG9186 ($C_0 = 2.06$) had the strongest affinity for the LD surface, compared with LSD1, and were not displaced from LDs even at the highest concentration of LSD1 (Figures 6B and S4A).

To further confirm these results, we performed a similar analysis using a *mCherry*-tagged form of the putative lipase CG9186 as a reference. These experiments yielded similar results (Figures 6C and 6D; Figures S4B and S4C). Importantly, at high expression levels, CG9186, like LSD1, displaced CCT1 and CG17292 from LDs. These results, in combination with the relative increase in concentration of CG9186 during lipolysis (Figures 1D and 1E), support the hypothesis that increased crowding at the LD surface is responsible for displacement of CCT1 and other proteins during lipolysis.

Lipid Droplet Binding Affinity Determines Localization during Lipolysis

If competition for the shrinking LD surface is a key determinant for LD protein composition during lipolysis, we hypothesized that the degree of displacement would inversely correlate with binding affinities at steady state. To evaluate this possibility, we defined a localization index for each protein. To calculate this index, we first compared the percentage of a protein on LDs with that elsewhere in the cell (Figure 2B) and normalized this ratio to the LD area to correct for effects of protein overexpression on LD abundance. Next, we calculated the fold change of protein on LDs after shrinkage compared with before lipid deprivation. The localization index is defined as the difference of the fold change from 1 (Figure 7A). Among the proteins analyzed, CCT1, CG17292, and FATP were reduced in concentration on LDs during shrinkage, reflected in a negative localization index. In contrast, ATGL, GPAT4, CGI-58, CG9186, and LSD1 increased in LD concentration, reflected in a positive localization index (Figure 7A).

For almost every protein tested, the localization index correlated strongly with the ability of each protein to compete for LD binding surface at steady state (Figure 7B). This suggests that the same fundamental principle—competition for limited binding sites on a crowded surface—underlies both protein displacement and LD localization at steady state. One exception is GPAT4, which was easily displaced by LSD1 but mostly remained bound after 24 hr of lipid deprivation. The explanation for this exception is currently unclear. We showed previously that GPAT4 is targeted to LDs via membrane bridges through an Arf1/COPI-dependent mechanism (Wilfling et al., 2013, 2014). It is therefore possible that LSD1 displaces targeting factors required for GPAT4 localization such as components of the Arf1/COPI machinery.

Our results suggest a model in which the binding of proteins to LDs is determined by their affinity for the LD surface, and that weakly associated proteins become displaced during lipolysis. To further test this idea, we increased the affinity of CCT LD-binding domain by fusing two copies of this domain (GFP-CCT1M_2; Figure 7C) and tested its behavior during lipolysis. As predicted, this construct has a higher affinity for the LD surface than one with a single M-domain according to FRAP analysis (estimated on-rate: 0.047/min versus 1.13/min for the single M-domain; Figures S5A and S5B). Furthermore, when co-expressed with LSD1, GFP-CCT1M_2 competed more efficiently for binding than the single M-domain (Figure 7D). To test whether this change in affinity leads to increased binding to the LD surface, we investigated the localization of both constructs during lipolysis. As predicted, GFP-CCT1M_2 remained on LDs to a greater extent than the single M-domain fusion (65% of the signal versus 20%) (Figures 7E and 7F). In addition, for both M-domain constructs, the localization index correlated with their binding affinity (Figure 7B).

DISCUSSION

Here, we show that macromolecular crowding is a major determinant of LD protein composition. During lipolysis, protein crowding alters LD composition by gradually expelling proteins

(C and D) High levels of CG9186 outcompete CCT at the surface of LDs. *mCherry*-CG9186 was co-expressed with GFP-CCT1 in LD-containing *Drosophila* S2 cells. (C) One representative cell with low expression (top) and one with high expression of LSD1 (bottom) are shown. LDs were stained with AUTOdot. Scale bar, 5 μm. Inlay, (D): mean fluorescence on LDs ± SD (n > 15). A.U., arbitrary units.
See also Figure S4.

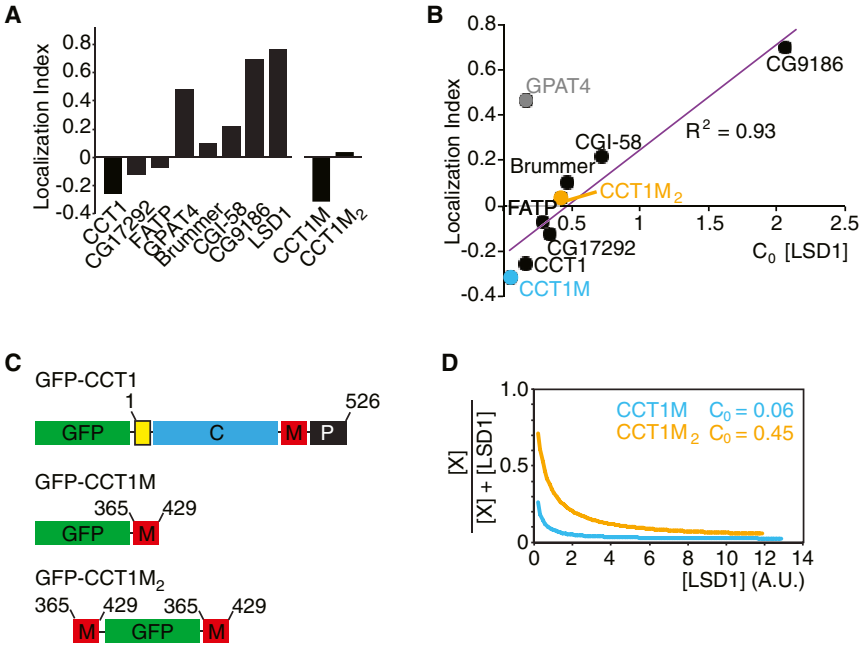

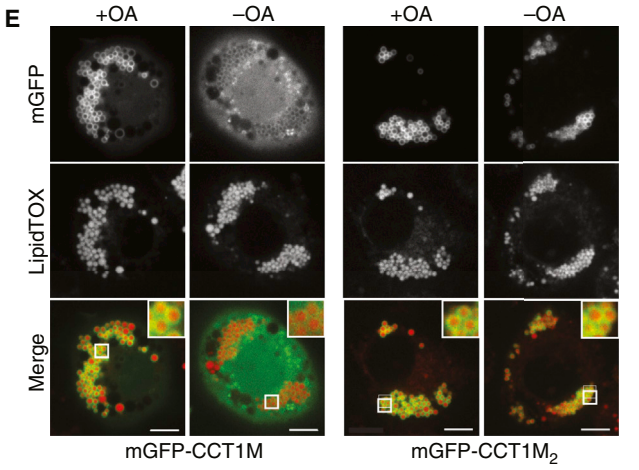

Figure 7. Binding Affinity Determines Protein Lipid Droplet Localization during Lipolysis

(A) LD proteins are displaced from LDs to different degrees during lipid starvation. The localization index is defined as the difference of the fold change in percentage of a protein on LDs versus the rest of the cell from 1.

(B) The correlation of localization index and critical LSD1 concentration needed to replace half of the amount of a bound protein from LDs as determined in Figure 6B. Linear regression, GPAT4 data were omitted from modeling.

(C) A schematic of GFP-tagged full-length CCT1, the LD binding domain (M-domain), and two copies of the M-domain.

(D) LSD1 displaces mGFP-CCT1M at a lower concentration than mGFP-CCT1M$_2$. A.U., arbitrary units.

(E and F) mGFP-CCT1M$_2$ falls off LDs less than mGFP-CCT1M. LDs were stained with LipidTOX. (E) Representative images are shown. Scale bar, 5 μm. Inlay: 3× magnification. (F) Mean fluorescence on LDs ± SD (n > 12). A.U., arbitrary units. See also Figure S5.

from their shrinking surfaces according to binding strength. Our in vitro studies show that this displacement occurs due to macromolecular crowding at the oil-water interface. Furthermore, when LD surfaces are at steady state, increasing levels of proteins with high LD binding affinity changes the LD protein composition, suggesting competition between proteins for the binding surface. Taken together, our results reveal a mechanism that governs the relative amounts of different LD proteins as they expand or contract.

The mechanisms regulating protein composition of LDs is apparently different from those that govern the composition of other membrane organelles, such as the ER, Golgi, or mitochondria. In the latter cases, protein composition is determined largely by expression and degradation of proteins, with signal sequences allowing import of proteins to the organelle (Nunnari and Walter, 1996). Alternatively, interactions of specific protein domains with highly enriched membrane lipid determinants, such as phosphoinositides, recruit proteins to these organelles. However, no such LD-specific determinants have been identified. Instead, we propose that the protein composition of LDs is determined in large part by competition for binding to limited sites on the monolayer surface. Because LDs exist as the dispersed oil phase of cellular emulsions, the available LD surface of individual droplets is coupled to the abundance of neutral lipids, limiting the possibilities for volume regulation that can occur with other organelles.

Macromolecular crowding is an important cellular phenomenon, influencing the behavior of bilayer membranes. At the plasma membrane, asymmetric protein crowding leads to membrane bending to release the lateral pressure (Derganc et al., 2013; Stachowiak et al., 2010, 2012). The effects of crowding differ in the case of LDs, where a surfactant monolayer covering a hydrophobic phase is more difficult to deform than a bilayer membrane (Thiam et al., 2013). In this situation, lateral pressure from crowding leads to displacement of proteins rather than bending of the surface. This response to crowding is similar to findings that were reported for surface proteins of plasma lipoproteins (Mitsche and Small, 2013).

From our study, two classes of LD proteins emerge with respect to the effects of crowding. One class, which includes CCT1, targets LDs from the cytoplasm and binds to LDs by inserting amphipathic helices into the surrounding monolayer. These proteins are the most susceptible to displacement due to crowding at the LD surface. A second class includes proteins with more hydrophobic helices that insert into the ER and subsequently re-localize to forming or expanding LDs (Ingelmo-Torres et al., 2009; Jacquier et al., 2011; Wilfling et al., 2013; Zehmer

et al., 2008). Generally, these hydrophobic proteins have higher LD binding affinities and are not crowded away from shrinking LDs during lipolysis. How cells remove these proteins from LDs when the droplets are entirely consumed is unclear.

Changes in monolayer lipid composition during lipolysis do not appear to contribute to displacement of weakly bound proteins, at least for CCT1. This contrasts with the binding of CCT1 to LDs, which is sensitive to PC deficiency and occurs during expansion to facilitate LD growth (Krahmer et al., 2011). Molecularly, the different sensitivity of CCT1 to surface lipids for binding versus displacement might be explained by the coupling of lipid binding to helix folding. When CCT binds to LDs, the folding of the amphipathic helical minimizes the energy penalty incurred by polar atoms being exposed to the hydrophobic environment of lipid side-chains. This step essentially renders the pathway of the binding reaction irreversible under these conditions (Antonny, 2011; Clayton et al., 2003). Therefore, CCT1 remains bound to the LD surface until proteins crowd, which increases collision events and causes its displacement from the surface.

Why some proteins are more easily displaced from the surface of LDs than others during crowding is an open question. One possibility is that the binding affinities of proteins targeted to LDs evolved due to selection pressures reflecting their functions in lipid storage or utilization. CCT1 provides an example. Previously, we showed that CCT1 exhibits a high apparent on-rate and binds tightly during LD expansion (Krahmer et al., 2011). Here, we show during lipolysis that CCT1 has a high propensity to fall off when LDs shrink, and CCT1 activity is no longer required. These properties reflect the need for CCT1 at the LD surface to provide PC during LD expansion, but not during LD shrinkage, when phospholipids are in excess and CCT1 activity is no longer required. Other proteins, such as lipase co-activator CGI-58 or the putative lipase CG9186, have a much lower propensity to be displaced by crowding, ensuring they stay on LDs during lipolysis. Such a mechanism for lipases may facilitate metabolic energy generation by optimizing substrate access during continued LD shrinkage.

Our findings do not exclude that processes other than crowding regulate LD composition. For example, the binding of some proteins, such as HSL, ATGL, CGI-58, and CCT1, is regulated by protein phosphorylation depending on metabolic state (Egan et al., 1992; Arnold et al., 1997; Brasaemle et al., 2000; Sahu-Osen et al., 2015; Xie et al., 2014). In addition, during LD expansion, surface lipid composition of LDs, such as deficiency of PC, influences the binding of CCT, and possibly of other LD proteins, to LDs to facilitate growth (Arnold et al., 1997; Jamil and Vance, 1990; Krahmer et al., 2011; Sletten et al., 2014). These mechanisms likely represent other layers of regulation that work in concert with protein crowding to control LD protein composition.

In conclusion, we propose that the unusual organelle structure of LDs—a monolayer interface and limited surface area—results in protein crowding serving as a general mechanism that determines their protein composition. As a mechanism, protein crowding may be advantageous to cells, as it enables the regulation of protein composition at the LD surface under changing conditions. For example, protein crowding may govern which proteins bind to LD surfaces during LD expansion versus shrinkage. According to this model, protein crowding would prevent proteins with weak affinities for membrane surfaces from binding to LDs during expansion. In this respect, PAT proteins, putative regulatory proteins found on most mammalian LDs, might serve such a crowding-related regulatory function. As we demonstrate, the PAT protein LSD1 has a high binding affinity for LDs and is efficient in competing other proteins off the LD surface. PAT proteins might therefore increase the stringency of proteins binding to LDs, effectively limiting binding to those proteins with relatively high affinity, thereby regulating the LD protein composition through a type of molecular proofreading.

EXPERIMENTAL PROCEDURES

Cell Culture and Transfection

Drosophila S2 cell culture and LD inductions were performed as described previously (Wilfling et al., 2013). For lipid starvation experiments, cells were treated with oleic acid overnight, washed in PBS three times, and incubated in media supplemented with 5% delipidated fetal bovine serum (Gemini Bio-Products). The medium was changed after 10, 24, and 32 hr. Lipolysis was blocked using the broad-specificity lipase inhibitor Orlistat (Cayman Chemical Company).

Fluorescence Microscopy

Immunofluorescence and spinning-disk confocal microscopy (100× 1.4 NA oil immersion objective [Olympus], iMIC [Till], CSU22 [Yokugawa], iXonEM 897 [Andor]) were performed as previously described (Wilfling et al., 2013). Primary antibodies against *Drosophila* CCT1, GPAT4 (Wilfling et al., 2013), or CG9186 (Thiel et al., 2013) and fluorescently labeled secondary antibodies (Life Technologies) were used. FRAP experiments were performed as described (Krahmer et al., 2011).

For co-expression competition experiments, *mCherry*- or GFP-tagged LD protein constructs in equal concentrations were transfected into S2 cells. After oleic acid treatment, cells expressing both proteins at various levels were imaged.

Image Quantification and Statistics

Images were analyzed using ImageJ software (Schneider et al., 2012). To determine the size of LDs, the diameters of the 20 largest LDs in 1 plane of the cell were measured. Small LDs were defined as less than 1.3 μm in size. To determine the LD area in one plane of the cell, Otsu thresholding was applied to the BODIPY channel and the resulting area was measured. For quantification of the %LD-targeted signal for a given protein, the image was background corrected and the total fluorescent signal on LDs was determined as a ratio to the total fluorescent signal in the whole cell. In co-expression experiments, the fluorescence signal on LDs was calculated by subtracting out the fluorescence signal elsewhere in each cell. Protein concentrations on LDs were derived from the mean fluorescence measured on LDs in each channel. Values from 15–20 cells were combined, and the standard deviation was calculated for statistical analysis.

Photoactivation Experiment

PAGFP-CCT1 (Patterson and Lippincott-Schwartz, 2002) was activated on LDs in a number of cells and imaged before and after 10 or 20 hr of lipid starvation. The integrated signal on LDs and the nucleus from 10 cells were combined for statistical analysis.

Curve Fittings

For the co-expression experiments, we determined the concentration of the protein on the basis of the mean fluorescence intensity, Prot, and the concentration of the reference protein, Protref (e.g., LSD1). To determine the fraction of displaced protein, we plotted Prot/(Prot+Protref) against Protref and fitted curves based on the function $1/(1+x/c_0)$ to the binned data, where x is the variable Protref and C_0 the concentration of *mCherry*-LSD1 at which half of the GFP-tagged protein is displaced from LDs (Protref = c_0). This fitting model is based on the Stoke-Einstein equation: when the protein concentration is

increased, the viscosity of the surface increased, which leads to impaired diffusion (diffusion D is inversely proportional to the viscosity). Since the amount of protein displacement correlated with surface diffusion (Figure 5E), we considered our fitting model adequate.

In Vitro Experiments

To purify LDs from cells expressing fluorescently tagged LD proteins, cells from 3–5 10-cm dishes were harvested, washed once in ice-cold PBS, and lysed using a 30G needle. To isolate LDs, cell lysates were mixed with 1 ml of 75% glycerol in Tris-buffered saline (TBS) buffer, overlaid with 1.5 ml of TBS, and spun at 100,000 × *g* for 1 hr. The top 750 μl were collected as the LD fraction. To create buffer-in-oil drops, a buffer-diluted LD fraction was mixed with triacylglycerol by vortexing to create buffer-in-oil drops.

For shrinking experiments, aqueous drops bounded by the triacylglycerol were imaged for 10 to 15 min on uncovered glass plates to allow for water evaporation. Where indicated, lipids (Avanti Polar Lipids) or PEG-C16 (TCI America) conjugates were added to the oil phase on the coverslips at 0.5% and 2% w/w, respectively, where indicated. Surfactant lipids were first dried under vacuum before being resuspended.

For the determination of the diffusion coefficient, we bleached part of the interface, in the in vitro experiments, of characteristic size l^2, and determined the characteristic recovery time t. The diffusion coefficient was estimated as l^2/t.

SUPPLEMENTAL INFORMATION

Supplemental Information includes five figures and can be found with this article online at http://dx.doi.org/10.1016/j.devcel.2015.06.007.

AUTHOR CONTRIBUTIONS

N.K., A.-R.T., and T.C.W. designed the research; N.K. and A.-R.T. performed research; N.K. and A.-R.T. analyzed data; N.K., A.-R.T., R.V.F., and T.C.W. interpreted results; and N.K., R.V.F., and T.C.W. wrote the paper.

ACKNOWLEDGMENTS

We thank Drs. Matthias Beller for the CG9186 antibody, Natalie Krahmer and Florian Wilfling for constructs, and Yi Guo for *mCherry*-LSD1. We also thank Drs. Thomas Melia, Niklas Mejhert, and Coline Prévost for comments and critical discussion and Dr. Michelle Pflumm and Gary Howard for editorial assistance. This work was supported by the Mathers foundation (T.C.W), the National Institute of General Medical Sciences (NIGMS) (R01GM-097194 to T.C.W; R01GM-099844 to R.V.F.), and the ATIP-Avenir program (A.-R.T.). In addition, A.-R.T held a Marie Curie Fellowship and N.K. an American Heart Association pre-doctoral fellowship.

Received: December 30, 2014
Revised: April 21, 2015
Accepted: June 8, 2015
Published: July 23, 2015

REFERENCES

Antonny, B. (2011). Mechanisms of membrane curvature sensing. Annu. Rev. Biochem. *80*, 101–123.

Arnold, R.S., DePaoli-Roach, A.A., and Cornell, R.B. (1997). Binding of CTP:phosphocholine cytidylyltransferase to lipid vesicles: diacylglycerol and enzyme dephosphorylation increase the affinity for negatively charged membranes. Biochemistry *36*, 6149–6156.

Arrese, E.L., Rivera, L., Hamada, M., Mirza, S., Hartson, S.D., Weintraub, S., and Soulages, J.L. (2008). Function and structure of lipid storage droplet protein 1 studied in lipoprotein complexes. Arch. Biochem. Biophys. *473*, 42–47.

Athenstaedt, K., and Daum, G. (1997). Biosynthesis of phosphatidic acid in lipid particles and endoplasmic reticulum of *Saccharomyces cerevisiae*. J. Bacteriol. *179*, 7611–7616.

Athenstaedt, K., Zweytick, D., Jandrositz, A., Kohlwein, S.D., and Daum, G. (1999). Identification and characterization of major lipid particle proteins of the yeast *Saccharomyces cerevisiae*. J. Bacteriol. *181*, 6441–6448.

Beller, M., Thiel, K., Thul, P.J., and Jäckle, H. (2010). Lipid droplets: a dynamic organelle moves into focus. FEBS Lett. *584*, 2176–2182.

Bigay, J., Casella, J.F., Drin, G., Mesmin, B., and Antonny, B. (2005). ArfGAP1 responds to membrane curvature through the folding of a lipid packing sensor motif. EMBO J. *24*, 2244–2253.

Brasaemle, D.L., Barber, T., Wolins, N.E., Serrero, G., Blanchette-Mackie, E.J., and Londos, C. (1997). Adipose differentiation-related protein is an ubiquitously expressed lipid storage droplet-associated protein. J. Lipid Res. *38*, 2249–2263.

Brasaemle, D.L., Levin, D.M., Adler-Wailes, D.C., and Londos, C. (2000). The lipolytic stimulation of 3T3-L1 adipocytes promotes the translocation of hormone-sensitive lipase to the surfaces of lipid storage droplets. Biochim. Biophys. Acta *1483*, 251–262.

Brasaemle, D.L., Dolios, G., Shapiro, L., and Wang, R. (2004). Proteomic analysis of proteins associated with lipid droplets of basal and lipolytically stimulated 3T3-L1 adipocytes. J. Biol. Chem. *279*, 46835–46842.

Clayton, A.H., Vultureanu, A.G., and Sawyer, W.H. (2003). Unfolding of class A amphipathic peptides on a lipid surface. Biochemistry *42*, 1747–1753.

Cui, H., Lyman, E., and Voth, G.A. (2011). Mechanism of membrane curvature sensing by amphipathic helix containing proteins. Biophys. J. *100*, 1271–1279.

Derganc, J., Antonny, B., and Copič, A. (2013). Membrane bending: the power of protein imbalance. Trends Biochem. Sci. *38*, 576–584.

Drin, G., Casella, J.F., Gautier, R., Boehmer, T., Schwartz, T.U., and Antonny, B. (2007). A general amphipathic α-helical motif for sensing membrane curvature. Nat. Struct. Mol. Biol. *14*, 138–146.

Dunne, S.J., Cornell, R.B., Johnson, J.E., Glover, N.R., and Tracey, A.S. (1996). Structure of the membrane binding domain of CTP:phosphocholine cytidylyltransferase. Biochemistry *35*, 11975–11984.

Egan, J.J., Greenberg, A.S., Chang, M.K., Wek, S.A., Moos, M.C., Jr., and Londos, C. (1992). Mechanism of hormone-stimulated lipolysis in adipocytes: translocation of hormone-sensitive lipase to the lipid storage droplet. Proc. Natl. Acad. Sci. USA *89*, 8537–8541.

Frick, M., Schmidt, K., and Nichols, B.J. (2007). Modulation of lateral diffusion in the plasma membrane by protein density. Curr. Biol. *17*, 462–467.

Fujimoto, Y., Itabe, H., Sakai, J., Makita, M., Noda, J., Mori, M., Higashi, Y., Kojima, S., and Takano, T. (2004). Identification of major proteins in the lipid droplet-enriched fraction isolated from the human hepatocyte cell line HuH7. Biochim. Biophys. Acta *1644*, 47–59.

Gong, J., Sun, Z., Wu, L., Xu, W., Schieber, N., Xu, D., Shui, G., Yang, H., Parton, R.G., and Li, P. (2011). Fsp27 promotes lipid droplet growth by lipid exchange and transfer at lipid droplet contact sites. J. Cell Biol. *195*, 953–963.

Goo, Y.H., Son, S.H., Kreienberg, P.B., and Paul, A. (2014). Novel lipid droplet-associated serine hydrolase regulates macrophage cholesterol mobilization. Arterioscler. Thromb. Vasc. Biol. *34*, 386–396.

Goose, J.E., and Sansom, M.S. (2013). Reduced lateral mobility of lipids and proteins in crowded membranes. PLoS Comput. Biol. *9*, e1003033.

Greenberg, A.S., and Coleman, R.A. (2011). Expanding roles for lipid droplets. Trends Endocrinol. Metab. *22*, 195–196.

Greenberg, A.S., Egan, J.J., Wek, S.A., Garty, N.B., Blanchette-Mackie, E.J., and Londos, C. (1991). Perilipin, a major hormonally regulated adipocyte-specific phosphoprotein associated with the periphery of lipid storage droplets. J. Biol. Chem. *266*, 11341–11346.

Grönke, S., Mildner, A., Fellert, S., Tennagels, N., Petry, S., Müller, G., Jäckle, H., and Kühnlein, R.P. (2005). Brummer lipase is an evolutionary conserved fat storage regulator in *Drosophila*. Cell Metab. *1*, 323–330.

Han, J., and Herzfeld, J. (1993). Macromolecular diffusion in crowded solutions. Biophys. J. *65*, 1155–1161.

Ingelmo-Torres, M., González-Moreno, E., Kassan, A., Hanzal-Bayer, M., Tebar, F., Herms, A., Grewal, T., Hancock, J.F., Enrich, C., Bosch, M., et al.

(2009). Hydrophobic and basic domains target proteins to lipid droplets. Traffic *10*, 1785–1801.

Jacquier, N., Choudhary, V., Mari, M., Toulmay, A., Reggiori, F., and Schneiter, R. (2011). Lipid droplets are functionally connected to the endoplasmic reticulum in *Saccharomyces cerevisiae*. J. Cell Sci. *124*, 2424–2437.

Jambunathan, S., Yin, J., Khan, W., Tamori, Y., and Puri, V. (2011). FSP27 promotes lipid droplet clustering and then fusion to regulate triglyceride accumulation. PLoS ONE *6*, e28614.

Jamil, H., and Vance, D.E. (1990). Head-group specificity for feedback regulation of CTP:phosphocholine cytidylyltransferase. Biochem. J. *270*, 749–754.

Krahmer, N., Guo, Y., Wilfling, F., Hilger, M., Lingrell, S., Heger, K., Newman, H.W., Schmidt-Supprian, M., Vance, D.E., Mann, M., et al. (2011). Phosphatidylcholine synthesis for lipid droplet expansion is mediated by localized activation of CTP:phosphocholine cytidylyltransferase. Cell Metab. *14*, 504–515.

Krahmer, N., Hilger, M., Kory, N., Wilfling, F., Stoehr, G., Mann, M., Farese, R.V., Jr., and Walther, T.C. (2013). Protein correlation profiles identify lipid droplet proteins with high confidence. Mol. Cell. Proteomics *12*, 1115–1126.

Kuerschner, L., Moessinger, C., and Thiele, C. (2008). Imaging of lipid biosynthesis: how a neutral lipid enters lipid droplets. Traffic *9*, 338–352.

Kurat, C.F., Natter, K., Petschnigg, J., Wolinski, H., Scheuringer, K., Scholz, H., Zimmermann, R., Leber, R., Zechner, R., and Kohlwein, S.D. (2006). Obese yeast: triglyceride lipolysis is functionally conserved from mammals to yeast. J. Biol. Chem. *281*, 491–500.

Mitsche, M.A., and Small, D.M. (2013). Surface pressure-dependent conformation change of apolipoprotein-derived amphipathic α-helices. J. Lipid Res. *54*, 1578–1588.

Nunnari, J., and Walter, P. (1996). Regulation of organelle biogenesis. Cell *84*, 389–394.

Paar, M., Jüngst, C., Steiner, N.A., Magnes, C., Sinner, F., Kolb, D., Lass, A., Zimmermann, R., Zumbusch, A., Kohlwein, S.D., and Wolinski, H. (2012). Remodeling of lipid droplets during lipolysis and growth in adipocytes. J. Biol. Chem. *287*, 11164–11173.

Patterson, G.H., and Lippincott-Schwartz, J. (2002). A photoactivatable GFP for selective photolabeling of proteins and cells. Science *297*, 1873–1877.

Pol, A., Gross, S.P., and Parton, R.G. (2014). Review: biogenesis of the multifunctional lipid droplet: lipids, proteins, and sites. J. Cell Biol. *204*, 635–646.

Sahu-Osen, A., Montero-Moran, G., Schittmayer, M., Fritz, K., Dinh, A., Chang, Y.F., McMahon, D., Boeszoermenyi, A., Cornaciu, I., Russell, D., et al. (2015). CGI-58/ABHD5 is phosphorylated on Ser239 by protein kinase A: control of subcellular localization. J. Lipid Res. *56*, 109–21.

Schneider, C.A., Rasband, W.S., and Eliceiri, K.W. (2012). NIH Image to ImageJ: 25 years of image analysis. Nat. Methods *9*, 671–675.

Sletten, A., Seline, A., Rudd, A., Logsdon, M., and Listenberger, L.L. (2014). Surface features of the lipid droplet mediate perilipin 2 localization. Biochem. Biophys. Res. Commun. *452*, 422–427.

Stachowiak, J.C., Hayden, C.C., and Sasaki, D.Y. (2010). Steric confinement of proteins on lipid membranes can drive curvature and tubulation. Proc. Natl. Acad. Sci. USA *107*, 7781–7786.

Stachowiak, J.C., Schmid, E.M., Ryan, C.J., Ann, H.S., Sasaki, D.Y., Sherman, M.B., Geissler, P.L., Fletcher, D.A., and Hayden, C.C. (2012). Membrane bending by protein-protein crowding. Nat. Cell Biol. *14*, 944–949.

Stone, S.J., Levin, M.C., and Farese, R.V., Jr. (2006). Membrane topology and identification of key functional amino acid residues of murine acyl-CoA:diacylglycerol acyltransferase-2. J. Biol. Chem. *281*, 40273–40282.

Thiam, A.R., Farese, R.V., Jr., and Walther, T.C. (2013). The biophysics and cell biology of lipid droplets. Nat. Rev. Mol. Cell Biol. *14*, 775–786.

Thiel, K., Heier, C., Haberl, V., Thul, P.J., Oberer, M., Lass, A., Jäckle, H., and Beller, M. (2013). The evolutionarily conserved protein CG9186 is associated with lipid droplets, required for their positioning and for fat storage. J. Cell Sci. *126*, 2198–2212.

Walther, T.C., and Farese, R.V., Jr. (2012). Lipid droplets and cellular lipid metabolism. Annu. Rev. Biochem. *81*, 687–714.

Wheeler, J.J., Wong, K.F., Ansell, S.M., Masin, D., and Bally, M.B. (1994). Polyethylene glycol modified phospholipids stabilize emulsions prepared from triacylglycerol. J. Pharm. Sci. *83*, 1558–1564.

Wilfling, F., Wang, H., Haas, J.T., Krahmer, N., Gould, T.J., Uchida, A., Cheng, J.X., Graham, M., Christiano, R., Fröhlich, F., et al. (2013). Triacylglycerol synthesis enzymes mediate lipid droplet growth by relocalizing from the ER to lipid droplets. Dev. Cell *24*, 384–399.

Wilfling, F., Thiam, A.R., Olarte, M.J., Wang, J., Beck, R., Gould, T.J., Allgeyer, E.S., Pincet, F., Bewersdorf, J., Farese, R.V., Jr., and Walther, T.C. (2014). Arf1/COPI machinery acts directly on lipid droplets and enables their connection to the ER for protein targeting. eLife *3*, e01607.

Wolins, N.E., Rubin, B., and Brasaemle, D.L. (2001). TIP47 associates with lipid droplets. J. Biol. Chem. *276*, 5101–5108.

Wolins, N.E., Brasaemle, D.L., and Bickel, P.E. (2006). A proposed model of fat packaging by exchangeable lipid droplet proteins. FEBS Lett. *580*, 5484–5491.

Xie, X., Langlais, P., Zhang, X., Heckmann, B.L., Saarinen, A.M., Mandarino, L.J., and Liu, J. (2014). Identification of a novel phosphorylation site in adipose triglyceride lipase as a regulator of lipid droplet localization. Am. J. Physiol. Endocrinol. Metab. *306*, E1449–E1459.

Zanghellini, J., Natter, K., Jungreuthmayer, C., Thalhammer, A., Kurat, C.F., Gogg-Fassolter, G., Kohlwein, S.D., and von Grünberg, H.H. (2008). Quantitative modeling of triacylglycerol homeostasis in yeast—metabolic requirement for lipolysis to promote membrane lipid synthesis and cellular growth. FEBS J. *275*, 5552–5563.

Zechner, R., Kienesberger, P.C., Haemmerle, G., Zimmermann, R., and Lass, A. (2009). Adipose triglyceride lipase and the lipolytic catabolism of cellular fat stores. J. Lipid Res. *50*, 3–21.

Zehmer, J.K., Bartz, R., Liu, P., and Anderson, R.G. (2008). Identification of a novel N-terminal hydrophobic sequence that targets proteins to lipid droplets. J. Cell Sci. *121*, 1852–1860.

Zimmerman, S.B., and Minton, A.P. (1993). Macromolecular crowding: biochemical, biophysical, and physiological consequences. Annu. Rev. Biophys. Biomol. Struct. *22*, 27–65.

Zimmermann, R., Strauss, J.G., Haemmerle, G., Schoiswohl, G., Birner-Gruenberger, R., Riederer, M., Lass, A., Neuberger, G., Eisenhaber, F., Hermetter, A., and Zechner, R. (2004). Fat mobilization in adipose tissue is promoted by adipose triglyceride lipase. Science *306*, 1383–1386.

PLOS | ONE

RESEARCH ARTICLE

The Energy of COPI for Budding Membranes

Abdou Rachid Thiam[1,2]*, **Frédéric Pincet**[1,2]*

1 Laboratoire de Physique Statistique, Ecole Normale Supérieure de Paris, Université Pierre et Marie Curie, Université Paris Diderot, Centre National de la Recherche Scientifique, 24 rue Lhomond, 75005, Paris, France, **2** Department of Cell Biology, School of Medicine, Yale University, 333 Cedar Street, New Haven, CT 06520, United States of America

* thiam@lps.ens.fr (ART); pincet@lps.ens.fr (FP)

Abstract

As a major actor of cellular trafficking, COPI coat proteins assemble on membranes and locally bend them to bud 60 nm-size coated particles. Budding requires the energy of the coat assembly to overcome the one necessary to deform the membrane which primarily depends on the bending modulus and surface tension, γ. Using a COPI-induced oil nanodroplet formation approach, we modulated the budding of nanodroplets using various amounts and types of surfactant. We found a Heaviside-like dependence between the budding efficiency and γ: budding was only dependent on γ and occurred beneath 1.3 mN/m. With the sole contribution of γ to the membrane deformation energy, we assessed that COPI supplies ~1500 k_BT for budding particles from membranes, which is consistent with common membrane deformation energies. Our results highlight how a simple remodeling of the composition of membranes could mechanically modulate budding in cells.

Citation: Thiam AR, Pincet F (2015) The Energy of COPI for Budding Membranes. PLoS ONE 10(7): e0133757. doi:10.1371/journal.pone.0133757

Editor: Ludger Johannes, Institut Curie, FRANCE

Received: February 9, 2015

Accepted: July 1, 2015

Published: July 28, 2015

Data Availability Statement: All relevant data are within the paper and its Supporting Information files.

Funding: This work was supported by International Outgoing Fellowship n° PIOF-GA-2011-299292 to ART.

Competing Interests: The authors have declared that no competing interests exist.

Introduction

Coat proteins, namely Clathrin coats, coat protein complex I (COPI) and II (COPII) perform a critical step of intracellular vesicle trafficking. They respectively form vesicles from the plasma, the Golgi and the endoplasmic reticulum membranes, exhibiting different morphology and mechanical properties. To induce vesicle formation, monomers of the coat protein machineries, called coatomers, assemble on the target membrane and polymerize to locally bud nanometer sized spherical caged-particles of given curvature [1, 2]. This budding process is biochemically and mechanically regulated [3, 4]. Biochemical regulation is inherent to local variation of one or several components of the coat protein machineries [4]. Mechanical regulation occurs by variations of the bending modulus κ, e.g. by remodeling of membrane composition, and the surface tension γ, e.g. by changing the membrane surfactant density [5, 6]. These mechanical parameters define the minimal energy for budding off a particle of radius r, $E = 8\pi\kappa+4\pi\gamma r^2$, the sum of the bending and stretching energies. This minimal energy which is presumably different for each organelle membrane has to be met by the polymerization energy of the coatomers, E^*, to form spherical coats enclosing the particles. Knowing E^* for each coat protein machinery will bring important and new knowledge on biochemical and biophysical regulation of cellular trafficking. Previous theoretical attempts based on the comparison

between the bending energy of bilayers and the elasticity of dilation of bilayer-bound coat proteins [7, 8] suggest E^* to be of the order of 2000 k_BT.

Of the three coat proteins, only COPI was shown to act *in vivo* on both phospholipid bilayers and monolayers, namely on the Golgi apparatus and lipid droplets which are organelles at the core of cellular energy metabolism [4, 9–11]. Because the Golgi has a very low surface tension γ ($<<1$ mN/m) [12], deforming its membrane is almost solely dependent on the bending modulus[13, 14] κ, ~20 k_BT, whose contribution to E is predominant. In contrast to the Golgi, lipid droplets are covered by a single phospholipid monolayer membrane. The surface tension of this type of membrane was determined for triolein emulsion droplets to be between 1 to 40 mN/m [5, 15], much higher than that of the Golgi bilayer. Hence, for lipid droplets, the contribution of γ becomes very important for the membrane deformation energy [5, 16].

The ability of COPI to bud nanoparticles from a monolayer or bilayer membrane can be predicted knowing E^{*COPI}, the energy supplied by the polymerization of COPI coatomers. Measuring E^{*COPI} in cells is experimentally challenging because the mechanical parameters are not controlled, membranes are dynamic systems and other proteins may interfere with them, and finally visualization of the coat formation is difficult. So far, various *in vitro* approaches, based on unilamellar vesicles [14, 17–19], or cell membrane extracts [20, 21], were used to exclusively study the ability of coat proteins to form vesicles. These approaches probed the biochemical triggering of budding and well described the molecular details of coatomer assembly mechanisms. The description of the energy landscape of the budding process is however still lacking because of the challenge to concomitantly visualize budded coat-vesicles with controlled membrane parameters.

Using a recently developed COPI-induced oil nanodroplet formation approach [5], we worked with different amounts and types of surfactant in the oil, to vary membrane mechanical properties, and studied how they influence nanodroplets budding. We found that the efficiency of the budding reaction depends on the surfactant type. However, a direct Heaviside-like dependence between the budding efficiency and γ was found, independently of the surfactant. Budding was mainly opposed by γ and occurred only beneath 1.3 mN/m. This simple dependency upon γ was expected for the emulsion monolayer membrane in our experiment because it was presumed that other mechanical terms have a minor contribution to budding. Hence, we used the sole contribution of the stretching energy due to γ to determine that COPI supplies an energy of ~1500 k_BT to bud membranes.

Materials and Methods

Preparation of the solutions

Phospholipids (PLs) and the triolein solution: we chose a lipid composition close to that of cellular natural lipid droplets [5]: Dioleoylphosphatidylcholine, Dioleoylphosphatidylethanolamine, Cholesterol, Lyso-Phosphatidylinositol, Lyso-Phosphatidylethanolamine, Lyso-Phosphatidylcholine (50:20:12:10:5:3). All phospholipids were purchased from Avanti Polar Lipids. The oil phase consisted of triolein (TO) purchased from Sigma Aldrich. The phospholipids were initially solubilized in chloroform that was first evaporated under vacuum. We then added the required amount of TO to the PLs to reach the desired concentration. The mixture was then vortex mixed for 2 min and subsequently sonicated for 1 min.

Cosurfactants (COs), Oleic acid (OA) and dioleoyl glycerol (DOG), were purchased from Sigma Aldrich.

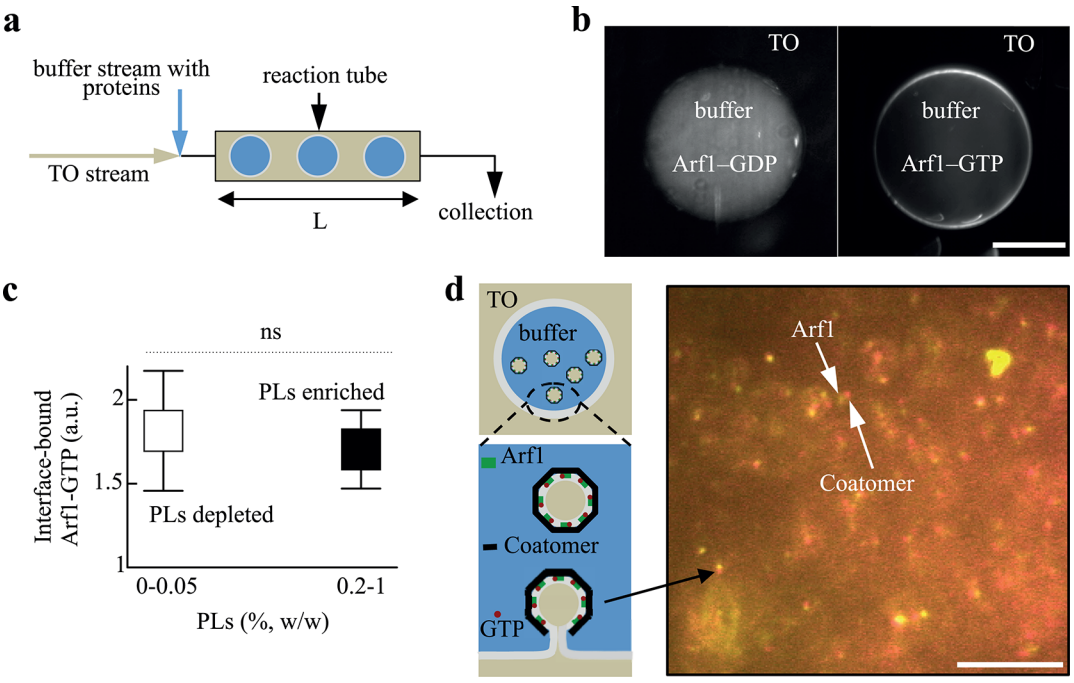

Fig 1. (a) Buffer drops formation. Triolein oil (TO) and buffer solutions were flown into a t-shape connector attached to a Teflon tube. Buffer drops encapsulating the proteins were formed in TO, inside the tube; they were collected from the tip of the tube for quantification. (b) Buffer drops containing Arf1-Cy3 (100 nM), in GTP (10 mM) or GDP bound form, and Arno (100 nM), were separately formed, arrested in the tube, and visualized by fluorescence. Arf1-GTP bound the interface (right panel); Arf1-GDP remained in volume (left). Scale bar is 100 μm. (c) Changing the amount of phospholipid (PL) did not impact the recruitment of Arf1-GTP to the interface. The ratios of Arf1-Cy3 signal between the membrane and the volume, with or without PLs (depleted, 0% PLs, enriched, 0.2% PLs (w/w to TO)) were similar; at 0.05% and 1%, the same trend was observed; about 20 drops were quantified for each case; the p-value is 0.3 and ns stands for non-specific. (d) Budding scheme of Arf1/COPI from the buffer/TO interface and visualization of a buffer microreactor content. The presence of colocalized Arf1-Cy3 (100 nM) and coatomer-Alexa647 (25 nM) spots reveals budding activity at the buffer interface as described in the scheme. Homogeneous particles (60 nm TO droplets) were budded inside the buffer drop as described in [5] and S1 Video. The frequent drift occurring between red and green signals is due to a time delay required for switching the lasers while particles were in motion in solution. Scale bar is 10μm.

doi:10.1371/journal.pone.0133757.g001

Generation of the buffer drops

The TO lipid oil and the buffer phase (50 mM Hepes, 120 mM Kacetate, and 1 mM $MgCl_2$ in MilliQ water) containing the proteins were stored into different syringes serving for injecting them in a T-connector attached to a Teflon tube (Fig 1A). Buffer drops were thus generated into the oil phase and arrested in the tube; they were then observed by fluorescence (Fig 1B–1D). When budding occurred, each buffer drop contained COPI-TO nanodroplets, which were collected at the tip of the Teflon tube and analyzed (Fig 1A and [5]).

Quantification of the budding process

Budded particles were collected after the budding reaction at the tip of the tube (Fig 1A). The collected sample was placed in a chamber whose bottom was made of glass, coated with a thin polydimethylsiloxane polymer layer (10 μm) to prevent sticking of the particles. Imaging of the particles was done using an inverted epifluorescence Zeiss microscope equipped with a 63x oil objective. To identify the budded particles, two emission channels were simultaneously recorded: TO labeled with Bodipy-green (from Lifetechnologies) and COPI (Alexa-647). The nanodroplets were identified as tiny particles having both markers. The budding process was quantified following our previous work [5]. For each probed membrane condition, we focused in the volume of the sample (focal depth 4 μm, field of view of 130 μm x 130 μm), took

snapshots every minute (ten times) and counted the number of protein-coated nanodroplets (e.g. Fig 2A); we changed the focal plan at least twice for each experiment. Finally, only fluorescence intensities of coatomer spots between 20–100% of the maximum coatomer signal in the focal plan were counted, as they corresponded to the most visible spots in the focal volume [5]; the laser power was kept constant.

We averaged the counted number of budded particles per area (130 μm x 130 μm) and determined their standard deviation. This number of budded particles per area is *a priori* dependent on the composition of the monolayer, cosurfactants (COs), phospholipids (PLs), and time, t; in the text, it is denoted n(COs,PL,t).

Surface tension measurements

Surface tension was measured using the drop weight method [22] and micropipette aspiration technique [5, 23]. These methods are described in our previous work [5].

Briefly, in the drop weight method, a buffer drop was continuously and slowly flown, at a flow rate of 20 μl/hr to allow dynamic interfacial equilibrium, in a TO oil phase containing a given concentration of surfactant. At a critical size it detaches. For each concentration, an image of the drop was taken every 5 sec. From the inner diameter d of the injection tube (d = 250 μm), the surface tension was given by $m^*g/(\pi^*d^*f)$ where f is a Wilkinson geometric parameter correction that depends on the ratio between d and the radius of the detached drop; g is the gravity constant. The mass m of the drop was calculated according to $m = v\Delta\rho$ (v is the drop volume and $\Delta\rho$ is the density difference between oil and buffer). Surface tension values measured by this method were in accordance with those obtained by the micropipette technique.

The device of the micropipette technique consisted of a micromanipulator and a pipette holder (Narishige). Pipettes were incubated in a 5% (wt/vol) bovine serum albumin solution before use, so as to prevent the adhesion of the droplets to the glass. Micromanipulation of a single droplet enabled determining the interfacial tension (γ) through measurement of the pipette radius, R_p, droplet radius, R_d, and the minimal aspiration pressure at which the droplet was drawn into the pipette, P_{suc}, following the equation:

$$\gamma = P_{suc}/(2(1/R_p - 1/R_d)).$$

The suction of the droplet was carried out using a syringe. The resulting pressure was measured with a pressure transducer (DP103; Validyne Engineering Corp.), the output voltage being monitored with a digital voltmeter. The pressure transducer (in the range of 55 kPa) was calibrated before experiments.

Results and Discussion

We recently developed an assay in which the COPI machinery acts on the monolayer of a buffer/TO interface, mimicking the surface of lipid droplets, to bud 60 nm-COPI-coated TO oil nanodroplets [5, 9]. In a basic microfluidic device, 200 μm-size buffer drops, encapsulating the COPI machinery, were generated in an environment consisting of a TO oil phase containing controlled amounts of phospholipids and/or other lipid surfactants (Fig 1A). As soon as the buffer microreactors were formed in the oil phase, a surfactant monolayer was bound to their interface. The properties of the monolayer remained constant during the experiments as the surrounding TO phase represents a reservoir of surfactants. We were able to show that the encapsulated COPI machinery uses this surfactant monolayer as a substrate to generate the 60 nm-COPI-coated TO particles (Fig 1D and S1 Video) which were confirmed by electron microscopy, fluorescence imaging, and fluorescence correlation spectroscopy [5].

To initiate the action of COPI machinery on a bilayer membrane, a small GTPase, ADP-ribosylation factor 1, Arf1, first strongly binds to the membrane, in presence of GTP and an exchange factor, e.g. Arno. For comparison, we observed that Arf1 also binds the buffer/TO monolayer interface in a GTP-specific manner (Fig 1B). The binding of the protein was moreover independent of the membrane composition (Fig 1C), as we varied over a wide range the surfactant concentration in the oil and observed no significant change in the amount of recruited protein. Based on this result, we considered that the contribution of Arf1 into the budding process was independent of membrane composition. Bound-Arf1 recruits coatomers that polymerize into a 60 nm-spherical cap enclosing TO particles ([5] and S1 Video). Since Arf1 recruitment did not depend on membrane composition, variation of the number of budded nanodroplets was exclusively assigned to the ability for COPI coatomers to fully polymerize in a spherical cap. Release of the budded particles in the microreactors requires the fission of the buds from the interface. Our study provides readout for both budding and fission together but can not discriminate between them. In the following, we will simply refer to nanodroplets formation, i.e. budding and fission, by budding.

The number of budded particles increases and saturates over time

We worked at 7 nM coatomer-Alexa647 and 100 nM Arf1 in the buffer microreactors, to make sure that, for each probed membrane condition, the kinetics of the proteins recruitment was not limiting, and that many nanodroplets will be formed under budding conditions. We generated buffer microreactors that were incubated for different times in the TO phase before collecting them. To achieve this, flow rates were kept constant (respectively at 1200 and 100 μl/h) and the length L of the reaction tube was varied (Fig 1A). In the TO oil phase, we varied the composition of the monolayer; it contained different concentrations of oleic acid (OA), dioleoylglycerol (DOG), phospholipids (PLs), or their combination. We did not see differences between OA and DOG in our experiments; when referring to both of them in the text we will use the annotation COs.

For each monolayer composition leading to budding, e.g. 1% PL (Fig 2B), the number of budded nanodroplets per area over time n(COs,PL,t) (see Materials and Methods and [5]) displayed a monotonic increase before reaching a plateau after 6 mins. The plateau or saturation of n(COs,PL,t) was expected because the concentration of free coatomers, which were consumed during budding, gradually decreased over time. For non-budding compositions, n(COs, PL,t) was zero even after 14 min reaction time, e.g. for 2% DOG or 0.1% PLs. We probed whether under these conditions budding could occur at longer time points. After 1h, having for example 1%, 2%, or 10% of COs in TO and/or less than 0.1% PLs, did not allow budding (Fig 2C); increasing the protein concentration by ten folds did not promote budding either after one hour. These results suggest that certain monolayer compositions were not favorable for budding, regardless of COPI concentration or how long the proteins were in contact with the monolayer. Conversely, budding was always observed in the presence of PLs at concentrations over 0.3% (Fig 2C).

Under budding conditions, we also observed different saturation levels of n(COs,PL,t), which were higher in the presence of 2% of COs for example (Fig 2A and 2B). In reality, COPI coatomers get inactivated after several minutes in solution, as they are formed by seven complexes that disassemble over time. This is the reason why we sought to work at high protein concentration to allow visualization of budding events despite disassembly and coatomer inactivation. The inactivation of the protein contributed of course to the saturation of budding but was essentially the reason for the difference observed between the saturation levels observed in

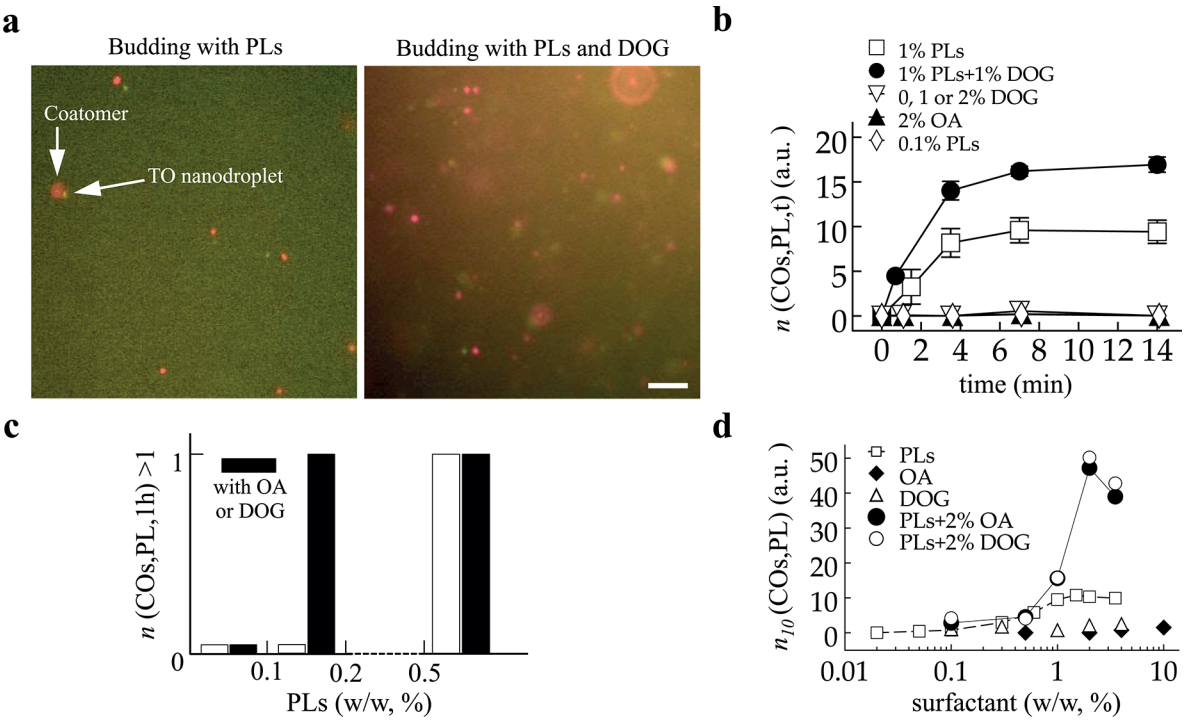

Fig 2. (a) Visualization of budded nanodroplets collected from microreactors after 10 min of reaction time. Coatomer and oil signals were recorded. Two cases of low and high COPI budding efficiency respectively due to the presence of low and high PL content with DOG (2%, w/w to TO) in TO. Scale bar is 10μm. (b) Evolution of the number of budded nanodroplets over time. Microreactors were collected at different time points and the number of budded nanodroplets per area *n*(COs,PL,t) was determined for various membrane conditions (e.g. 1% PLs or 2% DOG). Different plateaus were obtained for the two budding cases. (c) Occurrence of budding after one hour to visualize the non-budding/budding transition. When no budding was observed, the bar was set at zero; when *n*(COs,PL,1h) > 1 the bar was set at 1, independently of the value of *n* (COs,PL,1h). PL alone is represented in white bars. At 0.2% PLs and below, no budding occurred; at 0.5% PL and above budding occurred. Black bars correspond to the presence of COs in TO. Budding occurred only above 0.2%PL with 2% COs. The sole presence of 0, 1, 2, 10% of COs did not mediate budding at all after one hour reaction time. (d) Budding quantification after 10 min reaction time, n_{10}(COs,PL), for different formulations. The conditions are TO + 0 or 2% COs with various amounts of PLs, or TO in which the concentration COs was varied; the term surfactant refers to either PL or COs variation. COs alone did not allow budding. However, 2% COs increased the number of budded nanodroplets in presence of PLs.

doi:10.1371/journal.pone.0133757.g002

Fig 2B and visible in Fig 2D. Without the inactivation, we would expect both cases to reach the same plateau but at different time points.

In short, different parameters such as membrane composition for budding conditions and coatomer polymerization or disassembly affected the number of budded nanodroplets (Fig 2A and 2B). However, only membrane composition was responsible for the non-occurrence of budding, as increasing the concentration of proteins or reaction time did not promote budding (Fig 2C). Our results thus strongly suggest that regardless of time membrane composition was the key parameter determining budding occurrence, even though the number of formed nanodroplets may vary. This conclusion is valid as long as the reaction time is larger than the time scale of the full assembly of coatomers, which was of the order of a 1 minute as inferred from Fig 2B.

We conclude the existence of a budding transition dependent on membrane physical parameters. To investigate this transition, we varied the surfactant composition and concentration and determined n_{10}(COs,PL), the number of formed nanodroplets per area after 10 min of reaction time, as there were more particles to count. We determined n_{10}(COs,0%), n_{10}(0%,PL), n_{10}(2%,PL) and observed that having exclusively COs did not lead to particle formation by COPI (Fig 2D), regardless of their concentration, varied up to 10%, i.e. n_{10}(COs,0%) ~ 0. As

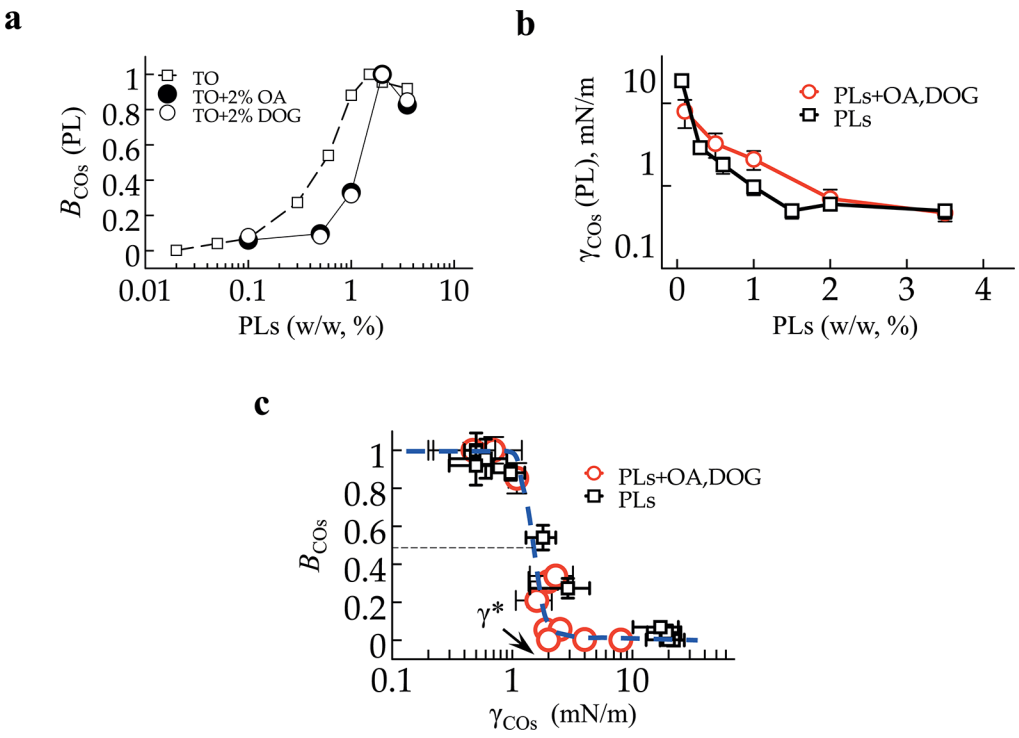

Fig 3. (a) For each budding formulation in Fig 2D, i.e. TO or TO + 2% COs with variable PL concentration, the budding efficiency $B_{COs} = n_{10}/\max(n_{10})$ was plotted. The transition of budding is shifted to higher PL concentrations in presence of COs. (b) The surface tension γ for each condition of (a) was measured; it exhibits an opposite variation to γ_{PL}, as there is a switch between circle and square symbols between (a) and (b). (c) The budding efficiency B_{COs} in logarithmic dependence of γ_{COs}. All data points follow a Heaviside-like master curve. The critical tension for budding is γ = 1.3 ± 0.2 mN/m.

doi:10.1371/journal.pone.0133757.g003

already shown [5], n_{10}(0%,PL) increased continuously up to 1% PL where it reached a maximum. Having additional 2% of OA or DOG as cosurfactants in TO increased n_{10}(2%,PL) compared to n_{10}(0%,PL). For example, by keeping the total surfactant amount at 4% in TO n_{10}(2%,2%) was five-fold larger than n_{10}(0%,4%) (Fig 2D). To understand these differences, mainly the effect of COs, we focused on COs = 0% and COs = 2% and used the normalized number of nanodroplets as B_0(PL) = n_{10}(0%,PL)/max(n_{10}(0%,PL)) and B_2(PL) = n_{10}(2%,PL)/max(n_{10}(2%,PL)). B_{COs} is defined as the budding efficiency for each COs concentration.

COPI budding efficiency is controlled by surface tension

We represented B_0 and B_2 (Fig 3A) against the PL concentration. We observed a shift of the budding efficiency profile of B_0(PL) towards higher phospholipid concentrations to obtain B_2(PL).

For the monolayer membrane of emulsion droplets, the surface tension γ is the relevant energy parameter of the membrane that may oppose the budding of nanodroplets. We measured γ_{COs}(PL) (Fig 3B) and observed that it evolved conversely to B_{COs}, and the shift observed in the presence COs was conserved (compare the position of circles and squares in Fig 3A and 3B). The surface tension increase of the PL monolayer owing to the presence of OA and DOG can be unexpected. In fact, OA and DOG are highly soluble in the TO oil phase, much more than PLs. Although they act as surfactants, they solubilize part of the PLs from the buffer/TO interface back into the oil, e.g. into micelles, thereby increasing surface tension, and vice versa. This probably explains the higher number of n_{10}(2%,2%) in Fig 2D compared to n_{10}(0%,4%).

Indeed, during budding, the PL monolayer of the microreactors is consumed by nanodroplets; for budding to continue, PLs in the TO have to quickly replenish the microreactors monolayer, which could have been facilitated by OA and DOG.

We represented B_{COs} against γ_{COs} and observed that all experimental data points follow a Heaviside-like master curve (Fig 3C) regardless of membrane composition. This supports our results (Fig 2B and 2C) that budding is either complete or never occurs for a given membrane composition in a time scale less than one hour. The budding efficiency consequently depended on the sole surface tension. Consistent with this finding, the exclusive modulation of vesicle budding by γ from giant unilamellar vesicles was shown [17].

The energy of COPI polymerization is ~1500–2000 k_BT

The required energy for nanodroplet formation can be written as the sum of bending and stretching energies, $E = 8\pi\kappa+4\pi\gamma r^2$. For emulsion droplets with fluid monolayer membranes, e.g. at the buffer/TO interface, the value of κ is generally beneath 10 k_BT [15, 24, 25]. In our experimental system, the contribution of 8πκ to the deformation energy would be thus constant and low, beneath 250 k_BT, while the contribution of the γ term was at least 1000 k_BT. The predominance of the stretching energy in our system explains the Heaviside-like dependence of budding with γ (Fig 3C) and offers a unique and simple way to assess E^{*COPI}. Continuously varying γ, by almost a hundred fold (Fig 3B and 3C), was de facto tuning the resistance of the membrane to deformation. Because budding occurred predominantly below 1 mN/m and was inexistent above 2 mN/m, with a sharp transition in between, we inferred the critical surface tension value, γ^*, beneath which COPI can form nanodroplets. The value of γ^* corresponds to the mid-point of the transition indicated in Fig 3C, corresponding to $\gamma^* = 1.3\pm0.2$ mN/m.

At the value of γ^*, E^{*COPI} and the nanodroplet formation energy, $4\pi\gamma^* r^2+8\pi\kappa$ are exactly balanced. The 60 nm-size budded nanodroplets have a 10 nm-thick coat [5, 18] and consequently an actual diameter of 2r = 40 nm. The stretching energy ($4\pi\gamma^* r^2$) was therefore ~1500 k_BT. By taking into account the bending energy (8πκ) which was a priori constant and lower than 250 k_BT, we found E^{*COPI} ~1500–2000 k_BT, in good agreement with previous theoretical predictions of less than 2000 k_BT [7, 8]. This value also suggests that in cells the largest bending modulus of a membrane which COPI can fully bud is $\kappa^* = E^{*COPI}/8\pi \sim 60\ k_BT$.

Potential mechanical and biochemical regulations of budding in cells

In a cellular context, the contributions of κ and γ evolve complexly due to frequent membrane remodeling. Mechanical regulation of budding by coat proteins means that membrane properties are dynamically adapted by cell activity between budding and non-budding physical states, based on E^{*COPI}.

For a monolayer membrane such as of lipid droplets, γ will essentially regulate the ability of COPI to perform budding, as a substantial increase of κ is unlikely [25]. The budding of COPI particles will for example quickly increase the surface tension of the monolayer, which will in return decrease and arrest the process when its value will be beyond γ^*. For the Golgi bilayer membrane, COPI mechanical regulation is more complex, as both contributions of κ and γ can be of similar importance. However, regulation by γ can be inferred from the occurrence of budding or fusion events of vesicles from/to a bilayer [14, 17], respectively inducing an increase or a decrease of the bilayer tension. This was well illustrated by the reconstitution of COPI vesicle budding from an initially deflated giant unilamellar vesicle (GUV) [17]. The budding of many vesicles resulted to an increase of the GUV surface tension, which arrested the process [17]. This control of budding by surface tension was well illustrated in cells by the gradual inhibition of COPI vesicle formation from swelling Golgi [26].

The value of E^{*COPI} also gives insights on the molecular dynamics of the coat proteins and their biochemical regulation. Forming a 60 nm-COPI coated particle involves n = 50 to 70 coatomers [27]. Each coatomer binds to 1 to 4 Arf1 proteins [4] and to 3 other coatomers [27]. The energy per bound-coatomer arising from the binding to Arf1 and to neighboring coatomers is $E^{*COPI}/n \sim 20–30\ k_BT$. This value is in good agreement with the prediction that vesicle budding should occur only if coatomers interaction overcomes $\kappa \sim 20\ k_BT$ [7, 8], the bilayer bending modulus. Assuming the binding to Arf1 do not have substantial contributions to budding, coatomer dimerization supplies an energy $e_d \sim 10\ k_BT$ corresponding to a lifetime $\tau = \tau_0 \exp(e_d/k_BT)$ (with $\tau_0 < 10^{-8}$s [28]) shorter than ~1 ms. With respect to organelles, this result shows that a COPI coat network will nucleate and grow only if several cascade of coatomer bonds are formed in less than 1 ms. The bond between two coatomers must be rapidly stabilized to prevent their disassembly. Stabilization of the forming spherical cap can be achieved by the rapid binding to other coatomers which is favored by increasing the coatomer concentration. In contrast, lowering the local COPI concentration, below a threshold at which the rate of coat bonds formation is slower than a few bonds per ms, will substantially prevent the coat growth [29]. Interaction of Arf1/coatomers with cargo receptors can also contribute to stabilize the emerging coat [4].

Conclusion

The emulsion-based approach presented here allowed us determining the COPI energy for budding membranes. Knowing this energy, which is ~1500–2000 k_BT, offers good projections on the mechanical and biochemical features of COPI coat assembly. Establishing the energies for other coat proteins would be of great interest to understand the difference and relevance between the molecular topologies of the proteins. These comparisons can be generalized to other proteins inducing membrane deformation such as Caveolins or BAR proteins. Knowing their energy value will bring considerable knowledge on the biological importance of membrane remodeling during cellular trafficking.

Supporting Information

S1 Video. Movie of the recovered budded oil nanodroplets. The product of the microreactors were recovered and placed between two cover slips. The oil signal is only shown. The nanodroplets are homogeneous. The number of nanodroplets decreased over time due to bleaching. The size of the field is 60 μm.
(AVI)

Acknowledgments

This work was supported by the Marie Curie "Budding and Fusion of Lipid Droplets" International Outgoing Fellowship within the 7th European Community Framework Program grant to A.R.T., a Partner University Funds exchange grant between the Yale and Ecole Normale Supérieure, and the ATIP-Avenir program grant to A.R.T. Authors greatly thank Dr. R. Beck for supplying proteins.

Author Contributions

Conceived and designed the experiments: ART FP. Performed the experiments: ART. Analyzed the data: ART FP. Contributed reagents/materials/analysis tools: ART FP. Wrote the paper: ART FP.

References

1. McMahon HT, Gallop JL. Membrane curvature and mechanisms of dynamic cell membrane remodelling. Nature. 2005; 438(7068):590–6. doi: 10.1038/nature04396 PMID: 16319878.
2. McMahon HT, Mills IG. COP and clathrin-coated vesicle budding: different pathways, common approaches. Curr Opin Cell Biol. 2004; 16(4):379–91. doi: 10.1016/j.ceb.2004.06.009 PMID: 15261670.
3. Sens P, Turner MS. Microphase separation in nonequilibrium biomembranes. Phys Rev Lett. 2011; 106(23):238101. PMID: 21770544.
4. Beck R, Rawet M, Wieland FT, Cassel D. The COPI system: molecular mechanisms and function. FEBS Lett. 2009; 583(17):2701–9. doi: 10.1016/j.febslet.2009.07.032 PMID: 19631211.
5. Thiam AR, Antonny B, Wang J, Delacotte J, Wilfling F, Walther TC, et al. COPI buds 60-nm lipid droplets from reconstituted water-phospholipid-triacylglyceride interfaces, suggesting a tension clamp function. Proc Natl Acad Sci U S A. 2013; 110(33):13244–9. doi: 10.1073/pnas.1307685110 PMID: 23901109; PubMed Central PMCID: PMC3746913.
6. Zimmerberg J, Kozlov MM. How proteins produce cellular membrane curvature. Nat Rev Mol Cell Biol. 2006; 7(1):9–19. doi: 10.1038/nrm1784 PMID: 16365634.
7. Chernomordik LV, Kozlov MM. Protein-lipid interplay in fusion and fission of biological membranes. Annu Rev Biochem. 2003; 72:175–207. doi: 10.1146/annurev.biochem.72.121801.161504 PMID: 14527322.
8. Kozlov MM, Chernomordik LV. The protein coat in membrane fusion: Lessons from fission. Traffic. 2002; 3(4):256–67. doi: 10.1034/J.1600-0854.2002.030403.X PMID: WOS:000174934100003.
9. Wilfling F, Thiam AR, Olarte M-J, Wang J, Beck R, Gould TJ, et al. Arf1/COPI machinery acts directly on lipid droplets and enables their connection to the ER for protein targeting. eLife. 2014; 3.
10. Guo Y, Walther TC, Rao M, Stuurman N, Goshima G, Terayama K, et al. Functional genomic screen reveals genes involved in lipid-droplet formation and utilization. Nature. 2008; 453(7195):657–61. Epub 2008/04/15. doi: 10.1038/nature06928 PMID: 18408709.
11. Beller M, Sztalryd C, Southall N, Bell M, Jackle H, Auld DS, et al. COPI complex is a regulator of lipid homeostasis. PLoS Biol. 2008; 6(11):e292. Epub 2008/12/11. doi: 10.1371/journal.pbio.0060292 PMID: 19067489.
12. Upadhyaya A, Sheetz MP. Tension in tubulovesicular networks of Golgi and endoplasmic reticulum membranes. Biophys J. 2004; 86(5):2923–8. doi: 10.1016/S0006-3495(04)74343-X PMID: 15111408; PubMed Central PMCID: PMC1304160.
13. Sens P, Johannes L, Bassereau P. Biophysical approaches to protein-induced membrane deformations in trafficking. Curr Opin Cell Biol. 2008; 20(4):476–82. doi: 10.1016/j.ceb.2008.04.004 PMID: 18539448.
14. Pinot M, Goud B, Manneville JB. Physical aspects of COPI vesicle formation. Molecular membrane biology. 2010; 27(8):428–42. doi: 10.3109/09687688.2010.510485 PMID: 21067455.
15. Kabalnov A, Tarara T, Arlauskas R, Weers J. Phospholipids as Emulsion Stabilizers: 2. Phase Behavior versus Emulsion Stability. Journal of colloid and interface science. 1996; 184(1):227–35. PMID: 8954658
16. Thiam AR, Farese RV Jr., Walther TC. The biophysics and cell biology of lipid droplets. Nat Rev Mol Cell Biol. 2013; 14(12):775–86. doi: 10.1038/nrm3699 PMID: 24220094.
17. Manneville JB, Casella JF, Ambroggio E, Gounon P, Bertherat J, Bassereau P, et al. COPI coat assembly occurs on liquid-disordered domains and the associated membrane deformations are limited by membrane tension. Proc Natl Acad Sci U S A. 2008; 105(44):16946–51. doi: 10.1073/pnas.0807102105 PMID: 18974217; PubMed Central PMCID: PMC2579358.
18. Faini M, Prinz S, Beck R, Schorb M, Riches JD, Bacia K, et al. The structures of COPI-coated vesicles reveal alternate coatomer conformations and interactions. Science (New York, NY. 2012; 336(6087):1451–4. doi: 10.1126/science.1221443 PMID: 22628556.
19. Saleem M, Morlot S, Hohendahl A, Manzi J, Lenz M, Roux A. A balance between membrane elasticity and polymerization energy sets the shape of spherical clathrin coats. Nat Commun. 2015; 6:6249. doi: 10.1038/ncomms7249 PMID: 25695735; PubMed Central PMCID: PMC4346611.
20. Ostermann J, Orci L, Tani K, Amherdt M, Ravazzola M, Elazar Z, et al. Stepwise assembly of functionally active transport vesicles. Cell. 1993; 75(5):1015–25. PMID: 8252615.
21. Wu M, Huang B, Graham M, Raimondi A, Heuser JE, Zhuang X, et al. Coupling between clathrin-dependent endocytic budding and F-BAR-dependent tubulation in a cell-free system. Nat Cell Biol. 2010; 12(9):902–8. doi: 10.1038/ncb2094 PMID: 20729836; PubMed Central PMCID: PMC3338250.

22. Yildirim OE, Xu Q, Basaran OA. Analysis of the drop weight method. Phys Fluids. 2005; 17(6). doi: 10.1063/1.1938227 PMID: WOS:000229749500009.

23. Yeung A, Dabros T, Masliyah J, Czarnecki J. Micropipette: a new technique in emulsion research. Colloids and Surfaces a-Physicochemical and Engineering Aspects. 2000; 174(1–2):169–81. doi: 10.1016/S0927-7757(00)00509-4 PMID: ISI:000089440200013.

24. Marsh D. Elastic curvature constants of lipid monolayers and bilayers. Chem Phys Lipids. 2006; 144 (2):146–59. doi: 10.1016/j.chemphyslip.2006.08.004 PMID: 17045578.

25. Kabalnov A, Wennerstrom H. Macroemulsion stability: The oriented wedge theory revisited. Langmuir. 1996; 12(2):276–92. doi: 10.1021/La950359e PMID: WOS:A1996TT76300009.

26. Takizawa PA, Yucel JK, Veit B, Faulkner DJ, Deerinck T, Soto G, et al. Complete vesiculation of Golgi membranes and inhibition of protein transport by a novel sea sponge metabolite, ilimaquinone. Cell. 1993; 73(6):1079–90. PMID: 8513494.

27. Lee C, Goldberg J. Structure of coatomer cage proteins and the relationship among COPI, COPII, and clathrin vesicle coats. Cell. 2010; 142(1):123–32. doi: 10.1016/j.cell.2010.05.030 PMID: 20579721; PubMed Central PMCID: PMC2943847.

28. Evans E. Probing the relation between force—lifetime—and chemistry in single molecular bonds. Annu Rev Biophys Biomol Struct. 2001; 30:105–28. doi: 10.1146/annurev.biophys.30.1.105 PMID: 11340054.

29. Foret L, Sens P. Kinetic regulation of coated vesicle secretion. Proc Natl Acad Sci U S A. 2008; 105 (39):14763–8. Epub 2008/10/01. doi: 10.1073/pnas.0801173105 PMID: 18824695.